

Development of Spleen Targeting H₂S Donor Loaded Liposome for the Effective Systemic Immunomodulation and Treatment of Inflammatory Bowel Disease

Chiwoo Oh, Wooseung Lee, Jeongbin Park, Jinyeong Choi, Somn Lee, Shengjun Li, Han Na Jung, Jeong-Seob Lee, Jee-Eun Hwang, Jiwoo Park, MinKyu Kim, Seungki Baek, and Hyung-Jun Im*



Cite This: <https://doi.org/10.1021/acsnano.2c08898>



Read Online

ACCESS |



Metrics & More



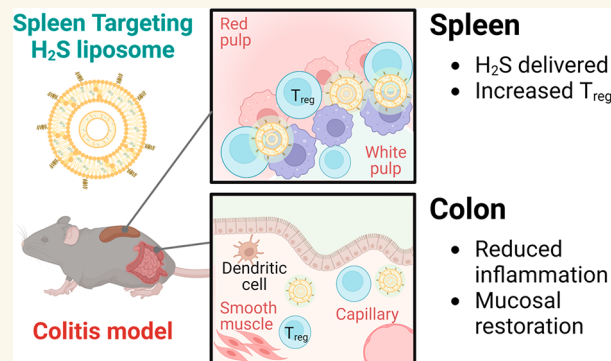
Article Recommendations



Supporting Information

ABSTRACT: Nanoparticles are primarily taken up by immune cells after systemic administration. Thus, they are considered an ideal drug delivery vehicle for immunomodulation. Because the spleen is the largest lymphatic organ and regulates the systemic immune system, there have been studies to develop spleen targeting nanoparticles for immunomodulation of cancer and immunological disorders. Inflammatory bowel disease (IBD) includes disorders involving chronic inflammation in the gastrointestinal tract and is considered incurable despite a variety of treatment options. Hydrogen sulfide (H₂S) is one of the gasotransmitters that carries out anti-inflammatory functions and has shown promising immunomodulatory effects in various inflammatory diseases including IBD. Herein, we developed a delicately tuned H₂S donor delivering liposome for spleen targeting (ST-H₂S lipo) and studied its therapeutic effects in a dextran sulfate sodium (DSS) induced colitis model. We identified the ideal PEG type and ratio of liposome for a high stability, loading efficiency, and spleen targeting effect. In the treatment of the DSS-induced colitis model, we found that ST-H₂S lipo and conventional long-circulating liposomes loaded with H₂S donors (LC-H₂S lipo) reduced the severity of colitis, whereas unloaded H₂S donors did not. Furthermore, the therapeutic effect of ST-H₂S lipo was superior to that of LC-H₂S lipo due to its better systemic immunomodulatory effect than that of LC-H₂S lipo. Our findings demonstrate that spleen targeting H₂S lipo may have therapeutic potential for IBD.

KEYWORDS: Spleen targeting, systemic immunomodulation, H₂S, liposome, inflammatory bowel disease



INTRODUCTION

Inflammatory bowel disease (IBD), which consists of ulcerative colitis and Crohn's disease, is characterized by a chronic incurable inflammatory process in the gastrointestinal tract with an uncertain pathophysiology.^{1,2} IBD is one of the growing global health problems with 6.8 million cases in 2017 globally, and its prevalence rate is increasing from 79.5 among 100,000 in 1990 to 84.3 among 100,000 in 2017.³ Although the mechanism of IBD has not been clearly identified, it is reported that abnormalities in immune regulation, genetic susceptibility, changes in the intestinal microflora, and environmental factors are associated with its pathophysiology.^{4,5} Therapeutic options for IBD include conventional anti-inflammatory agents such as 5-aminosalicylate, steroids, newer immunomodulatory agents such as tumor necrosis factor

(TNF)-alpha antagonist, anti-interleukin (IL) 23 and IL12 agents, and Janus kinase (JAK) inhibitors.⁶ These newer immunomodulatory agents have shown an efficacy in patients who did not respond to the conventional agents; however, the response rates have widely varied from 16–70% and 10–15% in patients who eventually underwent a colectomy due to refractory disease.⁷ Furthermore, these immunomodulatory

Received: September 6, 2022

Accepted: January 27, 2023

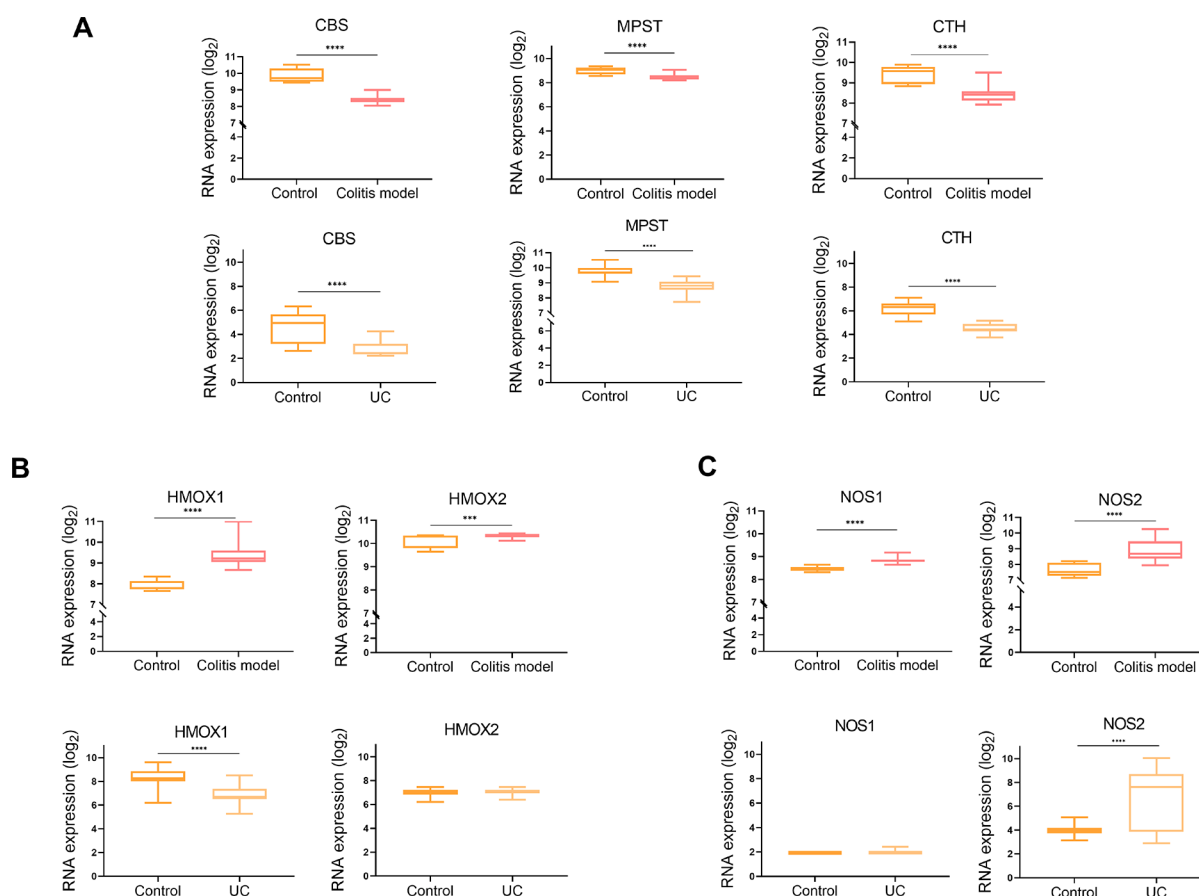


Figure 1. RNA expression analysis of enzymes related with gasotransmitters which are H₂S, NO, and CO in both DSS induced colitis model and ulcerative colitis patient. (A) The comparison of expression of H₂S related enzymes which are CBS, MPST, and CTH. The graphs of DSS colitis model (top) and ulcerative colitis patient (bottom) indicate quantified RNA expression differences. (B) The comparison of expression of NO related enzymes which are HMOX1 and HMOX2. The graphs of the DSS induced colitis model (top) and the ulcerative colitis patient (bottom) indicate RNA expression differences compared to the control group. (C) The comparison of expression of CO related enzymes which are NOS1 and NOS2. The graphs of the DSS induced colitis model (top) and the ulcerative colitis patient (bottom) indicate RNA expression differences compared to the control group. *: $P < 0.05$, **: $P < 0.01$, ***: $P < 0.001$. ****: $P < 0.0001$.

agents can increase the probability of opportunistic infections due to immune suppression.^{6,8–10}

Hydrogen sulfide (H₂S) is one of the endogenous gasotransmitters that involves various physiological processes.^{11,12} Because H₂S has a crucial role in the homeostasis of multiple physiological functions, abnormally decreased or increased H₂S levels are associated with multiple diseases including hypertension,¹³ atherosclerosis,¹⁴ diabetes,¹⁵ and gastrointestinal disorders.¹⁶ In particular, H₂S has pronounced anti-inflammatory and cytoprotective effects in the gastrointestinal tract. Therefore, H₂S donors are considered promising treatment agents in various gastrointestinal diseases. Additionally, several studies have demonstrated that a H₂S donor that escalates the H₂S level in tissues elicited notable therapeutic effects in a gastritis or colitis model.^{17–19} However, in previous studies, H₂S donors were administered directly as an experiment to demonstrate proof-of-concept for H₂S treatment, and studies on the development drug delivery systems for H₂S donors are lacking. An adequate drug delivery system for a H₂S donor is needed because direct administration has the following limitations: 1) it may not be suitable for clinical translation because local administration needs an expansive and cumbersome procedure such as endoscopy; 2) H₂S donors are not stable after they are dissolved in solution,

and 3) a systemic immunomodulation effect is less likely when it is administered locally.

The majority of nanoparticles that are systematically injected are captured by immune cells including macrophages, dendritic cells, and lymphocytes.^{20–22} Therefore, nanoparticles are considered highly suitable drug delivery vehicles for immunomodulation in various types of diseases. In particular, there have been studies utilizing spleen-targeting nanoparticles for immunomodulation²³ because the spleen is the largest lymphatic organ and modulates immune responses locally and systemically in the body.²⁴ For example, Zhai et al. developed a spleen targeting cancer nanovaccine based on the damaged membrane of red blood cells.²³ Additionally, Schmid et al. reported that anti-CD8 antibody labeled nanoparticles can be used as immune cell targeting delivery vehicles for cancer immunotherapy.²⁵

Here, we developed a H₂S donor, GYY4137, loaded spleen-targeting liposomes and tested their immunomodulatory properties in a dextran sulfate sodium induced mouse colitis model. Based on the anti-inflammatory effect of the H₂S donor and the intrinsic immune cell targeting ability of the nanoparticles, we hypothesized that 1) liposomal delivery of the H₂S donor would elicit a higher immunomodulation effect compared to the unloaded H₂S donor and that 2) delivery of

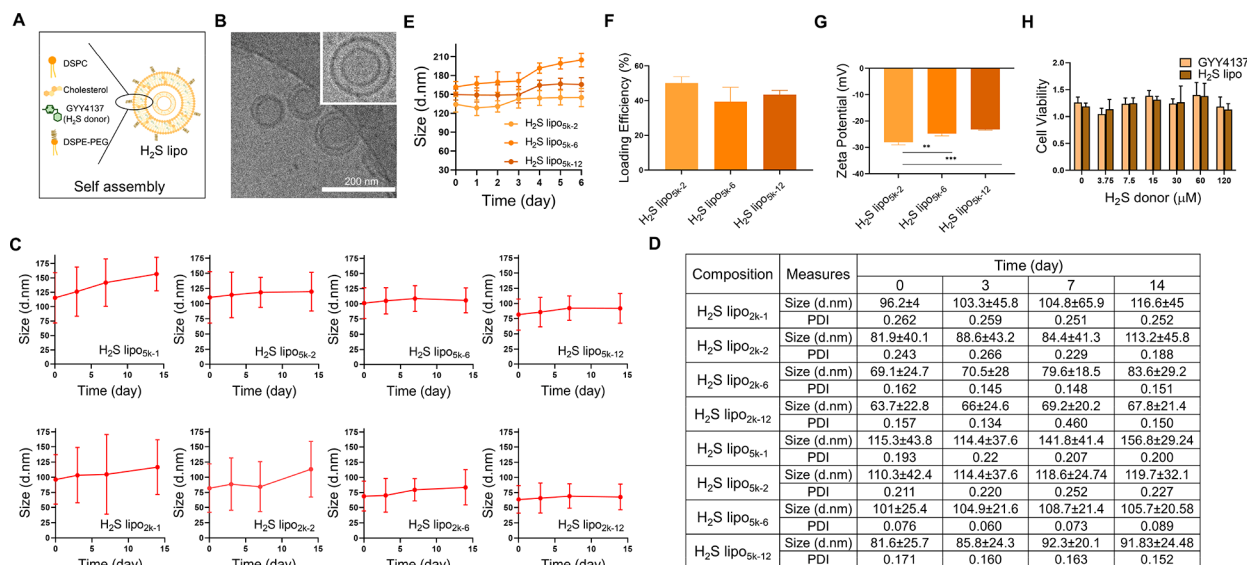


Figure 2. Characterization of H₂S liposome with different PEGylation strategies. (A) The schematic design of H₂S liposome composition (B) Cryo-TEM images of H₂S liposome. (C) The stability test of H₂S liposome with different PEGylation strategies. The stability of H₂S liposome was analyzed using size distribution profiles of DLS. The size distribution of H₂S liposome was acquired up to 14 days. (E) The stability test of H₂S liposomes in serum (D) The table of H₂S liposome stability test. The data of size and PDI according to composition are filled in the table up to 14 days. (F) The comparison of H₂S loading efficiency among different H₂S liposomes using the H₂S detection method ($n = 3$). (G) The comparison of surface net charge using zeta potential of DLS. (H) The cell viability test of H₂S liposome and GYY4137 using colorimetric MTT assay. Raw 264.7 cell line was used for MTT assay. The range of H₂S donor or H₂S liposome concentration is from 0 to 120 μ M. **: $P < 0.01$, ***: $P < 0.001$.

the H₂S donor using spleen-targeting liposomes would show a better immunomodulatory effect compared to the conventional long circulating liposome loaded H₂S donor.

RESULTS AND DISCUSSION

Transcriptomics-Level Evidence for the Potential of H₂S Based Therapeutics in Ulcerative Colitis. To explore the potential of H₂S based therapeutics in ulcerative colitis (UC), we examined the gene expression of H₂S synthesizing enzymes in patients with UC and in the mouse model of colitis. H₂S is synthesized by three enzymes, cystathionine-beta-synthase (CBS), cystathionine-gamma-lyase (CTH), and 3-mercaptopyruvate sulfurtransferase (MPST).²⁶ In both the UC patients and mouse model of colitis, gene expressions of H₂S synthesizing enzymes were significantly reduced compared to those of the normal control (Figure 1A) ($P < 0.0001$, all graphs). This observation could be one of the rationales to use H₂S donor therapeutics in UC patients. Meanwhile, the gene expression of the other gasotransmitters (NO and CO) synthesizing enzymes were not significantly decreased in colitis. In contrast to the H₂S synthesizing enzymes, the CO synthesizing enzymes, HMOX1 and HMOX2, showed a significantly higher expression in the colitis model compared to the control group ($P < 0.0001$, $P < 0.001$, respectively). In the UC patients, HMOX1 expression was significantly lower than in the control group, and HMOX2 expression was not significantly different compared to normal tissue ($P < 0.0001$) (Figure 1B). Moreover, the NO related enzymes, NOS1 and NOS2, showed an increased expression in the mouse colitis model compared to the control group (Figure 1C) ($P < 0.0001$, all graphs). Taken together, H₂S is the only gasotransmitter whose related genes are downregulated in both the mouse model of colitis and patients with UC.

Identification of Ideal Composition of H₂S liposome. We synthesized a H₂S donor, GYY4137, loaded liposome (H₂S

liposome) (Figure 2A, B). We tested various PEGylation strategies to develop the H₂S liposome with high stability and an efficient spleen targeting ability. Two types of 1,2-distearoyl-*sn*-glycero-3-phosphoethanolamine-polyethylene glycol (DSPE-PEG) (PEG: 2 kDa or 5 kDa) and four different mass ratios of distearoylphosphatidylcholine (DSPC) and DSPE-PEG (i.e., 1:12, 1:6, 1:2, and 1:1) were tested in the synthesis of the H₂S liposome. The four different mass ratios using 2 kDa PEG (i.e., 1:12, 1:6, 1:2 and 1:1) were named H₂S lip₀2k-1, H₂S lip₀2k-2, H₂S lip₀2k-6, and H₂S lip₀2k-12, respectively. The four groups using 5 kDa PEG (i.e., 1:12, 1:6, 1:2, and 1:1) were named H₂S lip₀5k-1, H₂S lip₀5k-2, H₂S lip₀5k-6, and H₂S lip₀5k-12, respectively. First, we tested the size stability of the various H₂S liposomes in distilled water (DW) at room temperature for 14 days using dynamic light scattering (DLS). We calculated the size changes of the H₂S liposomes between day 0 and day 14 to assess the degree of size stability, and the sizes of H₂S lip₀2k-1, H₂S lip₀2k-2, H₂S lip₀2k-6, H₂S lip₀2k-12, H₂S lip₀5k-1, H₂S lip₀5k-2, H₂S lip₀5k-6, and H₂S lip₀5k-12 were increased by 21.21%, 38.22%, 20.98%, 6.44%, 36%, 8.52%, 4.65%, and 12.53%, respectively (Figure 2C, D and Figure S1). We considered H₂S liposome groups with over a 20% size change as unstable forms of H₂S liposome. Additionally, H₂S lip₀2k-12 was the only H₂S liposome with 2 kDa PEG left; thus, we could not compare characteristics of the H₂S liposome with different 2 kDa PEG ratios. Therefore, H₂S lip₀5k-2, H₂S lip₀5k-6, and H₂S lip₀5k-12 were used in further characterization experiments. Then H₂S liposomes were tested stability in serum. We calculated the size change between day 0 and day 6. The size of H₂S lip₀5k-2, H₂S lip₀5k-6, and H₂S lip₀5k-12 were increased by 10.7%, 26.4%, and 11.2%, respectively (Figure 2E). The H₂S donor loading efficiency was tested by a precipitation method using silver nitrate (AgNO₃) (Figure S2A).²⁷ The detected optical density (OD) can be converted to the molar concentration using the weight concentration and molecular weight of

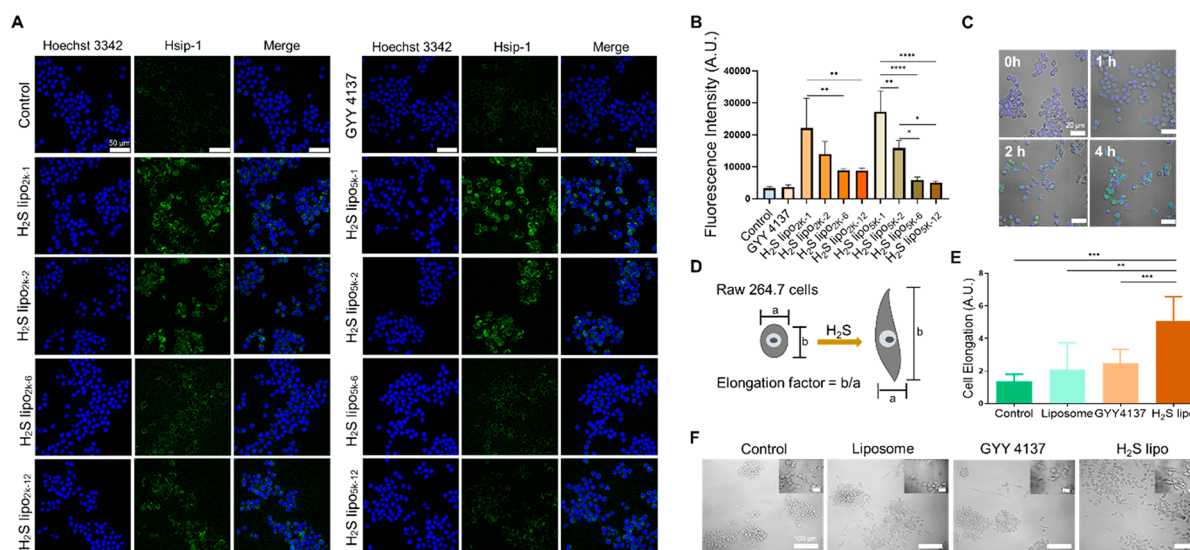


Figure 3. *In vitro* experiments of H₂S lipo. All *in vitro* experiments used macrophage cell line, RAW 264.7. (A) The fluorescence images of released H₂S by H₂S lipo after cell uptake. Hoechst 3342 was used for staining nucleic acid. Hsp-1 was used for detecting released H₂S by H₂S lipo after 1 h from adding reagents ($n = 4$). (B) The graph indicates the comparison of quantified fluorescence intensity among control, GYY 4137, and H₂S lipos. (C) The cell uptake images of H₂S lipo. FITC labeled H₂S lipo is used ($n = 6$). The confocal images were acquired at 0, 1, 2, and 4 h. (D) The schematic design of elongation factor analysis. (E) The graph indicates the comparison of quantified cell elongation factor among control, liposome, GYY 4137, and H₂S lipo ($n = 8$, respectively). (F) The comparison of M2 macrophage differentiation among bare liposome, GYY 4137, and H₂S lipo using morphological analysis ($n = 8$). *: $P < 0.05$, **: $P < 0.01$, ***: $P < 0.001$, ****: $P < 0.0001$.

GY4137 calculated from the standard curve (Figure S2B). There was no significant difference in the loading efficiency among the various H₂S lipos ($P = N.S.$) (Figure 2F). Next, the surface net charge was analyzed (Figure 2G). The zeta potential (mV) of H₂S lipo_{5k-2}, H₂S lipo_{5k-6}, and H₂S lipo_{5k-12} were -28.1 ± 0.9 , -24.8 ± 0.8 , and -23.2 ± 0.2 , respectively. The surface net charge of the H₂S lipo tended to increase as the mass of the PEG was increased (H₂S lipo_{5k-2} vs H₂S lipo_{5k-6}, $P < 0.01$; H₂S lipo_{5k-2} vs H₂S lipo_{5k-12}, $P < 0.001$ and H₂S lipo_{5k-6} vs H₂S lipo_{5k-12}, $P = 0.08$). Moreover, the loading stability test was confirmed with the H₂S detection method to identify whether the H₂S donor was well encapsulated and preserved in the H₂S lipo. We checked the percent change of the OD of GYY4137 and H₂S lipo_{5k-2} in DW for 8 days. The OD of GYY4137 increased over time up to 100% and was saturated at day 7; however, the OD of H₂S lipo_{5k-2} was only increased less than 10%, which indicated GYY4137 was stably loaded in the liposome. We speculated that GYY4137 is loaded in the hydrophobic layer of the liposome because GYY4137 releases H₂S in aqueous solution and does not release H₂S in a hydrophobic environment (Figure S2C). Taken together, the H₂S lipo is a drug delivery vehicle that could stably encapsulate the H₂S donor without any unwanted H₂S release.

Additionally, cell viability after treatment with GYY4137 and H₂S lipo was tested by MTT assay in RAW 264.7 cells. GYY4137 and H₂S lipo were not cytotoxic up to 120 μ M of GYY4137 (Figure 2H). In the cryogenic transmission microscopy (TEM) images, we identified that H₂S lipo_{5k-2} are uniformly shaped bilamellar liposomes (Figure 2B).

***In Vitro* H₂S Releasing and Immune Modulatory Effects of H₂S lipo.** When RAW 264.7 cells were treated H₂S lipos, they were able to release H₂S. We found that the H₂S releasing ability of H₂S lipo is superior to that of the unloaded H₂S donor, GYY4137. Moreover, as the PEG composition included in the H₂S lipo was decreased, more

H₂S release was detected (Figure 3A, B). However, H₂S lipo_{2k-1} and H₂S lipo_{5k-1} were not used for further experiments because they were unstable in the size stability test (Figure 2D). Additionally, further studies were done using H₂S lipo_{5k-2} because it has the highest degree of H₂S releasing ability among the stable H₂S lipos. In a cell uptake study, we found that a fluorescent H₂S lipo gradually was phagocytosed by RAW 264.7 cells over time (Figure 3C). In macrophage polarization, H₂S facilitates the production of peroxisome proliferator-activated receptor gamma (PPAR γ) and PPAR γ coactivator-1 β , resulting in inducing anti-inflammatory M2 macrophage.^{28,29} To assess the immunomodulatory effect of the H₂S lipo in RAW 264.7 cells, we calculated the elongation factor of the cells which is a phenotypic marker for anti-inflammatory M2 macrophages (Figure 3D).³⁰ H₂S lipo was able to induce macrophage elongation, and the degree of elongation was higher in the H₂S lipo treated cells compared to the control, liposome, and unloaded H₂S donor treated cells ($P < 0.001$, $P < 0.01$, $P < 0.001$, respectively) (Figure 3E, F). Also, we assessed mean fluorescence of intensity (MFI) of CD206 which is marker of the M2 macrophage using flow cytometry. Unlike unloaded GYY4137, the MFI of the H₂S lipo treated group was significantly more increased than that of the control group ($P < 0.01$) (Figure S11).

Assessment of the Spleen Targeting Ability of H₂S lipo. Positron emission tomography (PET) image based biodistribution analysis was done to assess the spleen targeting ability of H₂S lipo. We selected H₂S lipo_{5k-2}, H₂S lipo_{5k-6}, and H₂S lipo_{5k-12} to assess the spleen targeting ability because 1) PEG 2 kDa included H₂S lipos were more unstable compared to the PEG 5 kDa included ones, and 2) H₂S lipo_{5k-1} was unstable. PET has the advantage of showing the biodistribution of nanoparticles because it has excellent sensitivity and can detect an altered biodistribution by minor changes in the nanoparticles.³¹ To evaluate the appropriate PEGylation

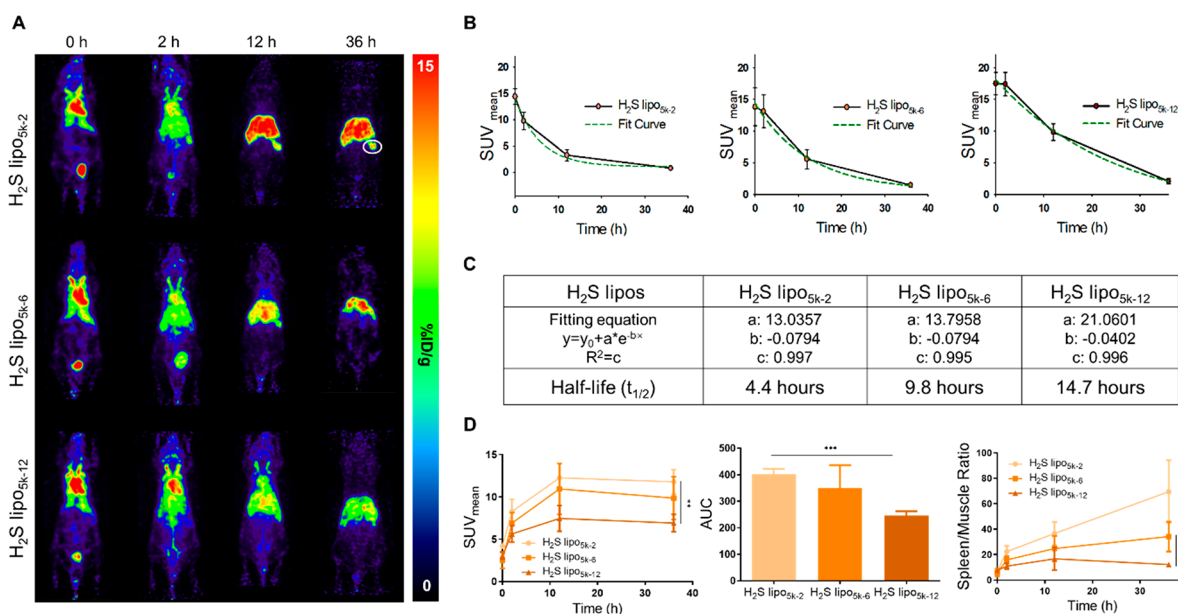


Figure 4. *In vivo* PET images of ^{64}Cu radiolabeled H₂S lipo. (A) The PET images were acquired using intravenously injected ^{64}Cu radiolabeled H₂S lipos which include H₂S lipo_{5k-2}, H₂S lipo_{5k-6}, and H₂S lipo_{5k-12} ($n = 3$, respectively). The time points of image acquisition are 0, 2, 12, and 36 h after injection. White circle indicates spleen. (B) The time activity curve graphs of blood pool and indicate circulation half-life. (C) The table of time activity curve data. The table includes fitting equation and half-life data. (D) The graph (left) indicates comparison of quantified spleen uptake. The graph (middle) indicates comparison of quantified AUC of spleen uptake graph. The graph (right) indicates comparison of quantified spleen/muscle ratio. *: $P < 0.05$, **: $P < 0.01$, ***: $P < 0.001$.

strategy for spleen targeting, we compared the *in vivo* biodistribution of ^{64}Cu radiolabeled H₂S lipo_{5k-2}, H₂S lipo_{5k-6} and H₂S lipo_{5k-12}. First, we investigated the radiolabeling efficiency and radiochemical stability using thin layer chromatography (TLC). Even after 24 h, the radiolabeling efficiency of H₂S lipo_{5k-2}, H₂S lipo_{5k-6} and H₂S lipo_{5k-12} remained 94.46%, 92.79%, and 95.74% in a phosphate buffered solution (PBS), confirming successful radiolabeling (Figure S3). From the *in vivo* biodistribution shown on the PET image, it was identified that H₂S lipo_{5k-2} rapidly accumulated in the spleen (Figure 4A). The circulation half-life of H₂S lipo_{5k-2}, H₂S lipo_{5k-6} and H₂S lipo_{5k-12} was 4.4, 9.8, and 14.7 h, respectively, making H₂S lipo_{5k-12} suitable for a long circulating liposome loaded H₂S donor (Figure 4B, C). In the standard uptake value (SUV_{mean}) graph, which quantitatively calculated the H₂S lipos targeted to the spleen, the SUV_{mean} of H₂S lipo_{5k-2} was significantly higher than that of H₂S lipo_{5k-12} ($P < 0.001$). In the area under curve (AUC) of the SUV_{mean} graph, the AUC of H₂S lipo_{5k-2} was significantly higher than that of H₂S lipo_{5k-12} ($P < 0.001$). In the spleen to muscle ratio, H₂S lipo_{5k-2} was significantly more accumulated than that of H₂S lipo_{5k-6} and H₂S lipo_{5k-12} ($P < 0.05$, $P < 0.05$, respectively) (Figure 4D). We found a simple PEGylation strategy suitable for spleen-targeting by quantitatively analyzing the PET images and designated H₂S lipo_{5k-2} as a spleen-targeting H₂S lipo (ST-H₂S lipo) and H₂S lipo_{5k-12} as a long-circulating H₂S lipo (LC-H₂S lipo).

We also tested whether ST-H₂S lipo successfully delivers H₂S donors to the spleen (Figure S4). We intravenously injected saline, GYY4137, and ST-H₂S lipo each into mice. Next day, the mice were euthanized, and the spleens were collected. The extracted spleens were homogenized and reacted with AgNO_3 . After the reaction, the spleen sample from the ST-H₂S lipo injected mice showed the darkest color and the highest OD among the compared groups (Figure S4B,

C), which confirmed that ST-H₂S lipo can efficiently deliver H₂S donors to the spleen. Furthermore, we studied whether the delivered H₂S to the spleen affects the differentiation of immune cells using flow cytometry (Figure S4D). We observed changes in the differentiation of regulatory T cells (T_{reg} , $\text{CD45}^+\text{FOXP3}^+\text{CD4}^+$ T cells) among the splenocyte population. The ST-H₂S lipo injected group showed more T_{reg} differentiation than that of the saline and GYY4137 injected groups ($P < 0.01$ and $P < 0.001$, respectively) (Figure S4E). We were able to quantitatively identify a PEGylation strategy suitable for spleen targeting through the PET images. In the *in vivo* experiments, ST-H₂S lipo showed a significant accumulation and H₂S release ability in the spleen. In addition, ST-H₂S lipo successfully induced T_{reg} differentiation in the spleen compared to the unloaded H₂S donor. These results suggest the potential of the immunomodulatory function of ST-H₂S lipo and lead us to the next experiment.

In Vivo Biodistribution of H₂S lipo in a Colitis Model.

Before we moved on to examine the therapeutic effect of H₂S lipo in a DSS-induced colitis model, we evaluated the biodistribution of ST-H₂S lipo and LC-H₂S lipo in the model. H₂S lipo as a versatile platform could signal fluorescence through the intercalation of DiR which is the one of the fluorescent dyes. Saline, DiR, DiR labeled ST-H₂S lipo, and DiR labeled LC-H₂S lipo were each systemically administered into the colitis model. Organs were removed after 24 h, and fluorescence images were obtained. We hypothesized that ST-H₂S lipo accumulates in the spleen, and LC-H₂S lipo accumulates more in the inflamed site of the colon due to a longer circulation time. As expected, ST-H₂S lipo showed prominent uptake in the spleen while LC-H₂S lipo showed minimal uptake ($P < 0.0001$). In the colon, both LC-H₂S lipo and ST-H₂S lipo accumulated in the colon, and the uptake was significantly higher for LC-H₂S lipo compared to ST-H₂S lipo ($P < 0.0001$) (Figure 5). Consequently, we identified that the

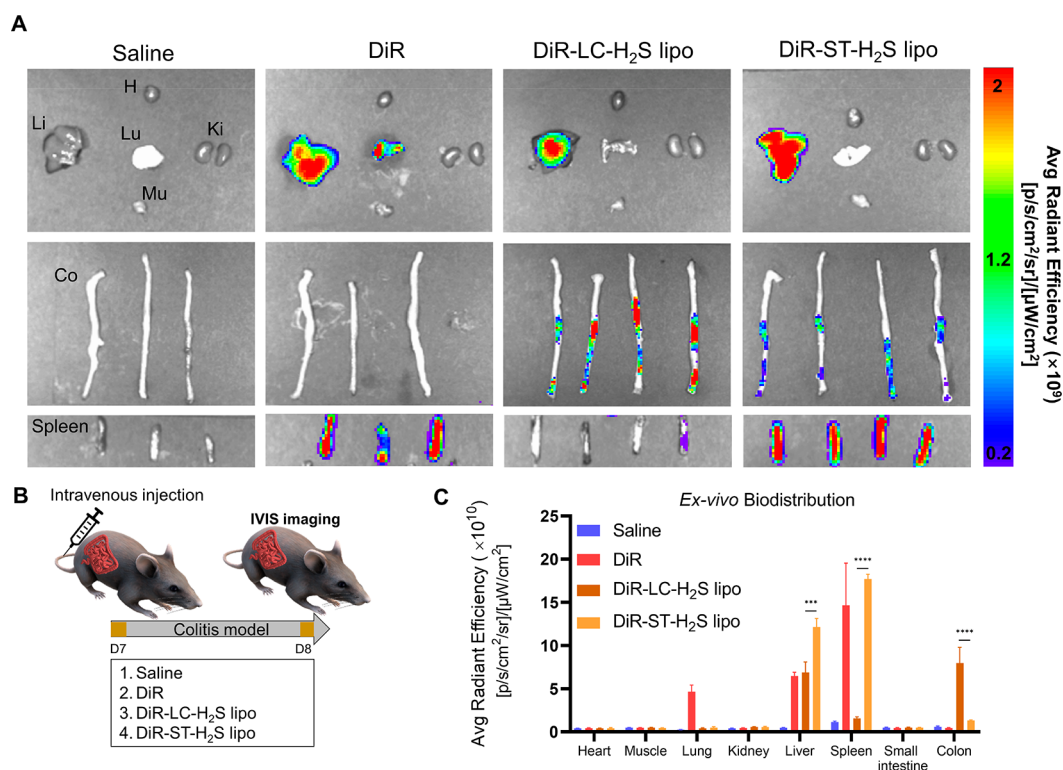


Figure 5. *Ex vivo* biodistribution in DSS induced colitis model. (A) Biodistributions of saline injected group, DiR injected group, DiR-LC-H₂S lipo injected group, and DiR-ST-H₂S lipo injected group were compared ($n = 3$; saline and DiR, $n = 4$; DiR-LC-H₂S lipo, DiR-ST-H₂S lipo). The *ex vivo* fluorescence images showed organs which are heart (h), liver (Li), lung (Lu), kidney (K_i), muscle (Mu), colon (Co), and spleen. Organs were collected after 24 h intravenously injection. *Ex vivo* fluorescence images were acquired by IVIS. (B) The schematic design of *ex vivo* biodistribution imaging in DSS induced colitis model. CS7BL/6 mice were induced colitis using 3% DSS (36–50 kDa). (C) The graph indicates comparison of quantified average radiant efficiency of extracted organs among saline, DiR, DiR-LC-H₂S lipo, and DiR-ST-H₂S lipo. ***: $P < 0.001$. ****: $P < 0$.

PEGylation strategies of H₂S lipo could be suitable for systemic or local immunomodulation in the colitis model. ST-H₂S lipo demonstrated an excellent spleen targeting ability and a moderate targeting ability to inflammatory sites which therefore may elicit a systemic and local immunomodulatory effect. Meanwhile, LC-H₂S lipo may be suitable for delivery of H₂S to an inflamed site due to its long-circulating property.

We further explored the splenic distribution of H₂S lipo through analysis using microscopic fluorescent H₂S lipo and H&E images. We systemically administrated DiD labeled ST-H₂S lipo in normal mice ($n = 3$). After 24 h, spleens were extracted and used for the analysis. As expected, the fluorescence intensity was not shown in the control mouse. The fluorescence signals of DiD labeled ST-H₂S lipo were well aligned with the histological structures of the spleen. Our evaluation of the fluorescence signal intensity in the different parts of the spleen (white pulp, red pulp, and marginal zone) showed that the marginal zone had the highest intensity, followed by the red pulp and the white pulp. This led us to speculate that ST-H₂S lipo may modulate the activity of various immune cells in the marginal zone, resulting in an immunomodulatory effect (Figure S14).

Therapeutic Effect of H₂S lipo in the Colitis Model. First, the therapeutic effect of the H₂S lipo and unloaded H₂S donor was compared in the DSS-induced colitis model (Figure 6A). We daily intravenously injected GYY4137 (60 μ M), GYY4137 (100 μ M), ST-H₂S lipo (60 μ M), and ST-H₂S lipo (100 μ M) each. The weights change (%) between day 0 and day 11 for the normal, saline, GYY4137 (60 μ M), GYY4137

(100 μ M), ST-H₂S lipo (60 μ M), and ST-H₂S lipo (100 μ M) treated groups were $104.57 \pm 4.3\%$, $71.84 \pm 5.85\%$, $73.62 \pm 3.01\%$, $73.34 \pm 8.41\%$, $77.80 \pm 4.15\%$, and $82.52 \pm 10.28\%$, respectively. Only the ST-H₂S lipo (100 μ M) treated group showed a statistically significant less weight reduction compared to the saline treated DSS colitis model (Repeated Measure Analysis Of Variance, Tuckey posthoc test, $P = 0.032$) (Figure 6B). The degree of inflammatory process for each group was observed with H&E stained slides of the colon epithelium. In the saline treated DSS-induced colitis models, the epithelial structure was almost entirely destroyed, and immune cells were massively infiltrated. In the GYY4137 (100 μ M) treated models, although the mucosal structures were slightly more preserved compared to the saline treated model, mucosal ulcerations were found. Moreover, immune cells were infiltrated into level of the muscularis mucosa. Interestingly, the ST-H₂S lipo (100 μ M) treated models showed a preserved mucosa structure with intact goblet cells, and only a small number of immune cells were infiltrated (Figure 6C). Inflammation scores were measured with the H&E slides and compared among the groups. The GYY4137 treated models showed a significantly lower score than that of the saline treated model ($P < 0.01$). The ST-H₂S lipo (100 μ M) treated group showed a significantly lower score than those of the saline and GYY4137 (100 μ M) treated groups ($P < 0.0001$ and $P < 0.05$, respectively) (Figure 6D). Furthermore, alcian blue staining of the colon epithelium was performed to evaluate the mucin component after treatment. The GYY4137 treated models tended to preserve mucin to some extent, unlike the

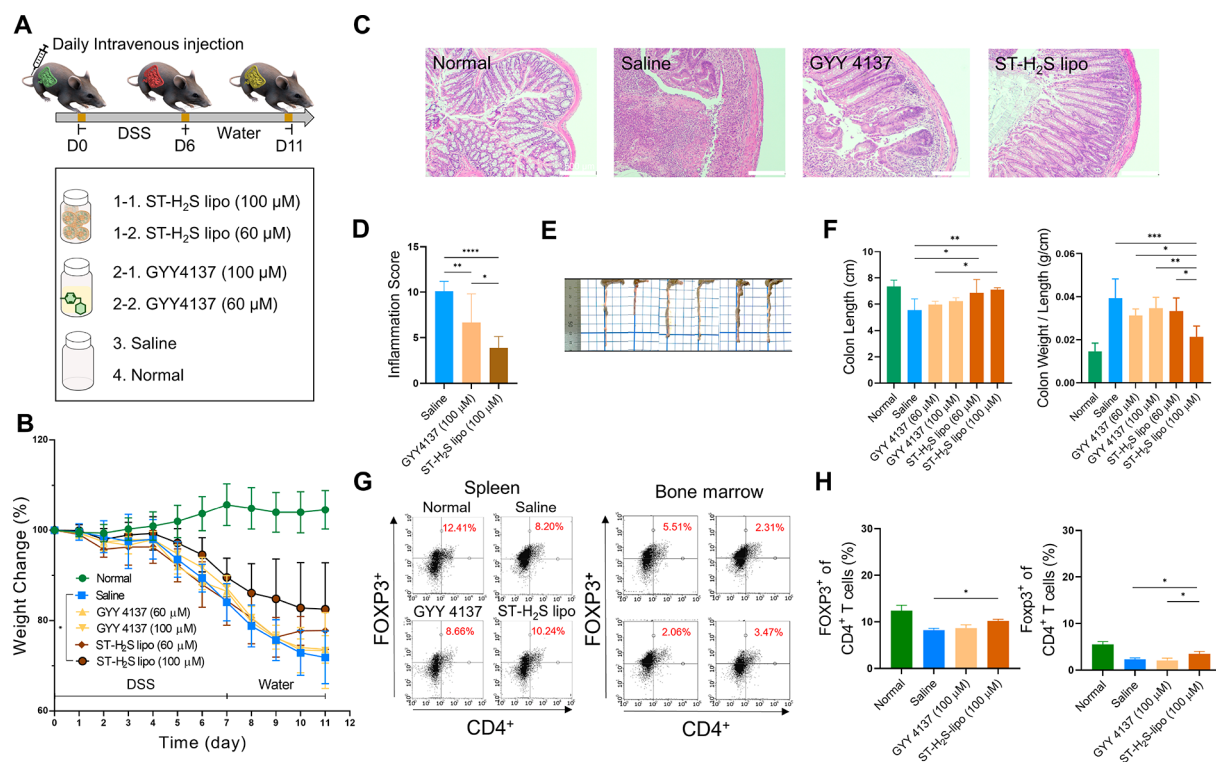


Figure 6. Comparison of therapeutic effect between normal, saline, GYY4137, and H₂S lipo in DSS induced colitis model. (A) The schematic design of therapeutic experiments in DSS induced colitis model. C57BL/6 mice were induced colitis using 3% DSS (36–50 kDa). Reagents and saline are daily intravenously injected. (B) The graph indicates comparison of weight change ($n = 5$, respectively). Weight change (%) shows the change based on 0 day. (C) The H&E images of colon of colitis model. (D) The graph indicates comparison of inflammation score ($n = 8$, respectively). (E) The representative images of extracted colon in colitis model. (F) The graph (left) indicates comparison of colon length ($n = 5$, respectively). The graph (right) indicates comparison of colon weight/length ($n = 5$, respectively). (G) The dot plot of flow cytometry. CD4 and FOXP3 antibodies are used as T_{reg} cell marker. (H) The graph (left) indicates comparison of quantified FOXP3⁺ of CD4⁺ T cells (%) in spleen ($n = 3$). The graph (right) indicates comparison of FOXP3⁺ of CD4⁺ T cells (%) in bone marrow ($n = 3$). *: $P < 0.05$, **: $P < 0.01$, ***: $P < 0.001$. ****: $P < 0.0001$.

saline treated models in which the mucin component was barely detected ($P = 0.14$). The ST-H₂S lipo (100 μ M) treated group showed a significantly higher alcian blue intensity than that of the saline treated group ($P < 0.5$) (Figure S5). In terms of colon length, only the ST-H₂S lipo group showed significantly less contraction of the colon compared to the saline group (ST-H₂S lipo (60 μ M), $P < 0.05$; ST-H₂S lipo (100 μ M), $P < 0.01$). In terms of colon weight and length which reflect the degree of inflammation of the colon, we identified that the ST-H₂S lipo (100 μ M) treated model had a significantly lower value compared to the saline, GYY4137 (60 μ M), GYY4137 (100 μ M), and ST-H₂S lipo (60 μ M) treated models ($P < 0.001$, $P < 0.05$, $P < 0.01$, and $P < 0.05$, respectively) (Figure 6E, F). To explore the systemic immune modulation effect, the T_{reg} proportion was evaluated in bone marrow and spleen samples after treatment (Figure S6). The ST-H₂S lipo (100 μ M) treated group showed more T_{reg} differentiation than that of the saline treated group in the spleen ($P < 0.05$). Additionally, the ST-H₂S lipo (100 μ M) treated group showed more T_{reg} differentiation of bone marrow compared to the saline and GYY4137 (100 μ M) treated groups ($P < 0.05$, $P < 0.05$, respectively) (Figure 6G, H). To sum up, we identified that ST-H₂S lipo showed a higher therapeutic effect than that of the unloaded H₂S donor in the DSS induced colitis model. ST-H₂S lipo was able to induce T_{reg} differentiation in the spleen and bone marrow.

We further explored the therapeutic effects of ST-H₂S lipo and LC-H₂S lipo in the DSS induced colitis model. The weight change (%) at 10 days for the normal, saline, ST-H₂S lipo, and LC-H₂S lipo groups was 102.61 ± 4.63 , 75.62 ± 3.34 , 84.16 ± 8.39 , and 76.33 ± 7.76 , respectively (Figure 7A, B). The ST-H₂S lipo treated group showed a significantly less weight change compared to the saline treated control group (Repeated Measure Analysis Of Variance and Tuckey posthoc test, $P = 0.02$). However, the LC-H₂S lipo treated group showed no significant difference in weight change compared to the saline treated control group ($P = \text{N.S.}$) (Figure 7B). In the H&E staining, both the ST-H₂S lipo and LC-H₂S lipo treated groups showed less immune cell infiltration and epithelial destruction compared to the saline treated control group (Figure 7C). Moreover, ST-H₂S lipo had a lower inflammation score compared to the saline and LC-H₂S lipo treated groups ($P < 0.0001$, $P < 0.01$; respectively) (Figure 7D and Figure S7). In the comparison of the colon length, only the ST-H₂S lipo treated group showed significant differences compared to the saline treated group ($P < 0.05$). For the colon weight and length, the ST-H₂S lipo treated group had a significantly lower colon weight and length compared to the saline treated group ($P < 0.05$) (Figure 7E, F). To assess the systemic immune modulation effect, differentiation of T_{reg}, M1, and M2 macrophages in the spleen was evaluated using flow cytometry. Unlike LC-H₂S lipo, ST-H₂S lipo significantly induced more T_{reg} differentiation than that of the saline group ($P < 0.05$).

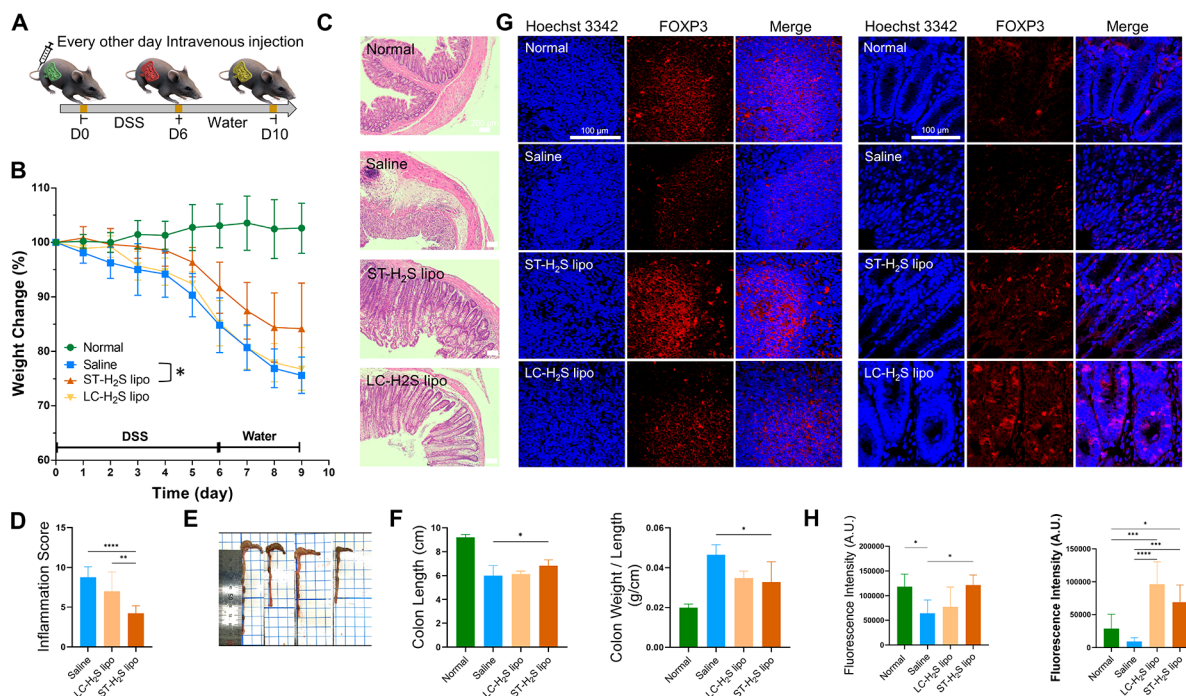


Figure 7. Comparison of therapeutic effect between normal, saline, ST-H₂S lipo, LC-H₂S lipo in DSS induced colitis model. (A) The schematic design of therapeutic experiments in DSS induced colitis model. C57BL/6 mice were induced with colitis using 3% DSS (36–50 kDa). Reagents were intravenously injected every other day. (B) The graph indicates comparison of weight change between normal, saline, ST-H₂S lipo, and LC-H₂S lipo. (C) The H&E images of colon of colitis model. (D) The graph indicates comparison of inflammation score between saline, ST-H₂S lipo, and LC-H₂S lipo ($n = 8$). (E) The extracted images of colon in colitis model. Representative images indicate normal, saline, ST-H₂S lipo, and LC-H₂S lipo from left, respectively. (F) The graph (left) indicates comparison of colon length ($n = 5$, respectively). The graph (right) indicates comparison of colon weight/length ($n = 5$, respectively). (G) Confocal images of FOXP3 differentiation in spleen (left) and colon (right). Red fluorescence by Cyanine5.5 indicates FOXP3 of T_{reg} cells. (H) The graph (left) indicates comparison of fluorescence intensity in spleen ($n = 5$). The graph (right) indicates comparison of fluorescence intensity in colon ($n = 5$). *: $P < 0.05$, **: $P < 0.01$, ***: $P < 0.001$, ****: $P < 0.0001$.

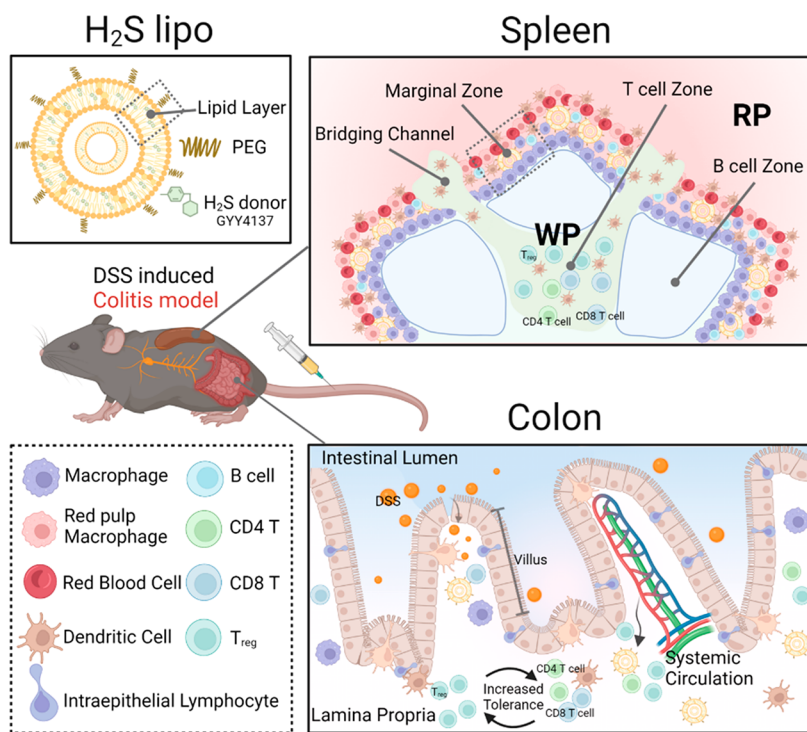


Figure 8. Schematic illustration of the H₂S lipo treatment in DSS induced colitis model. Immune responses according to H₂S lipo of spleen and colon are illustrated. DSS: dextran sulfate sodium, WP: white pulp, RP: red pulp.

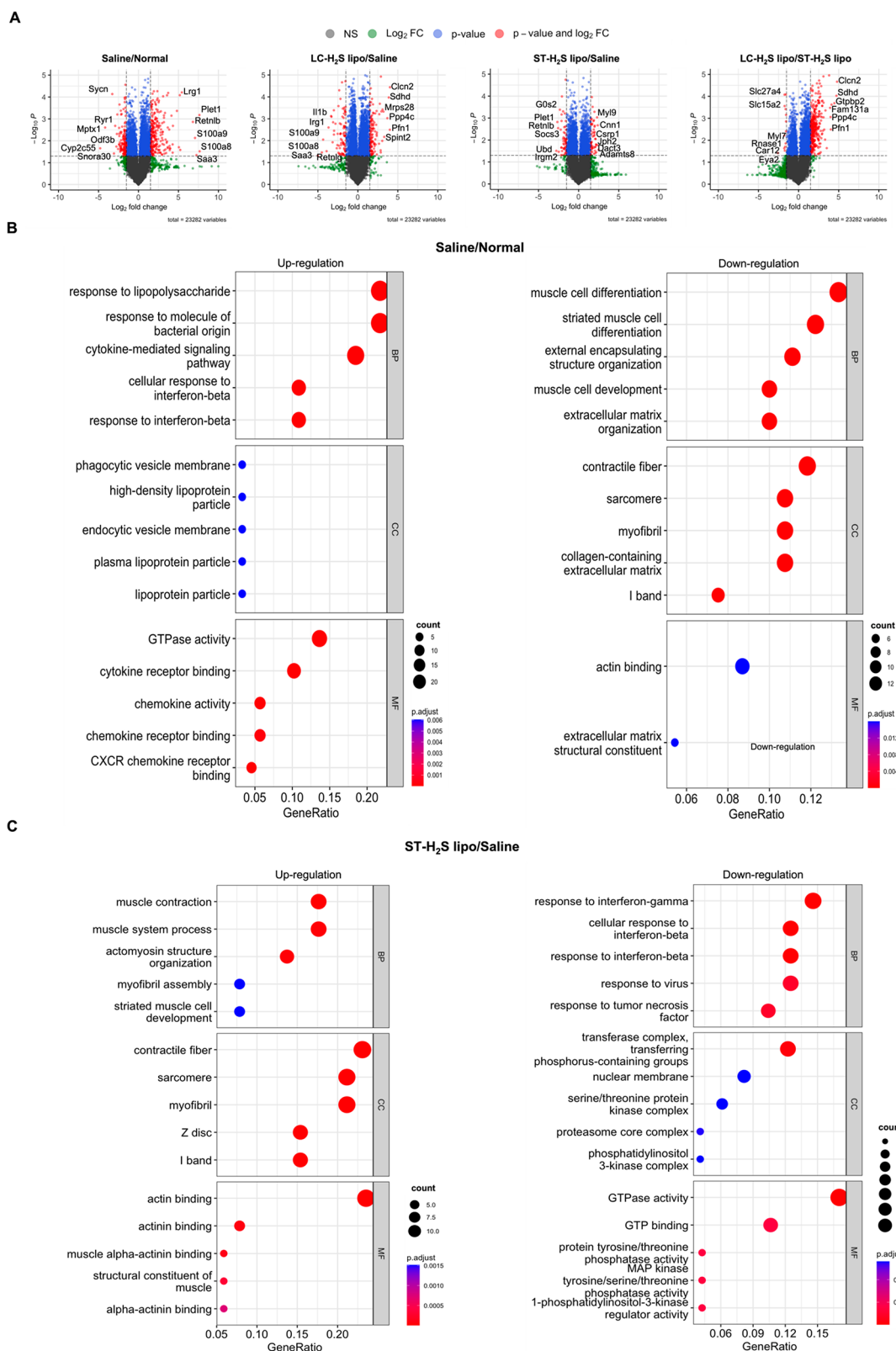


Figure 9. RNA-seq analysis of immunomodulatory process by H₂S lipos in DSS induced colitis model. (A) Volcano plots for the comparison of a pair of groups in bulk RNA-seq analysis. A pair of groups is saline vs normal, LC-H₂S lipo vs saline, ST-H₂S lipo vs saline, and LC-H₂S lipo vs ST-H₂S lipo. A total of 23,282 genes were plotted in each plot. (B) The GO analysis of a pair of groups in bulk RNA-seq data. A pair of groups is saline vs normal. (C) The GO analysis of a pair of groups in bulk RNA-seq data. The pair of groups is ST-H₂S lipo vs saline.

The ST-H₂S lipo treated group tended to have less M1 differentiation (F4/80⁺ CD80⁺) compared to the saline treated group ($P = 0.053$). Additionally, the ST-H₂S lipo treated group

tended to have higher M2 (F4/80⁺ CD206⁺) differentiation compared to the saline treated group ($P = 0.15$) (Figure S8). In spleen and mucosal tissues, T_{reg} differentiation was assessed

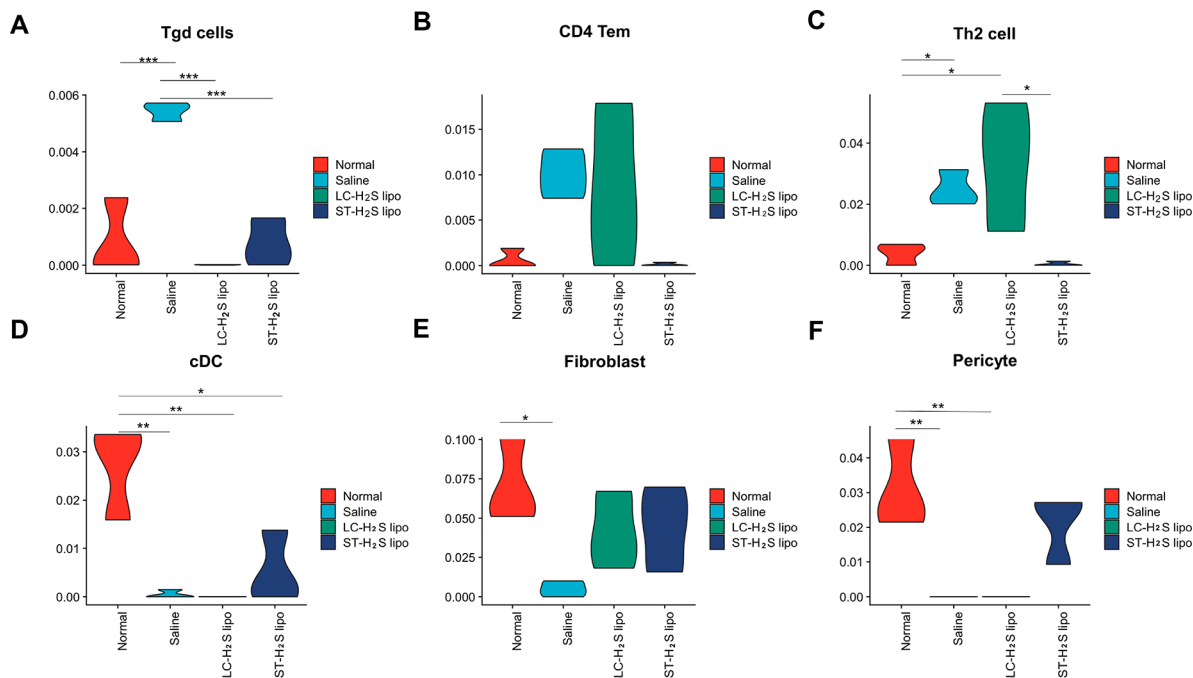


Figure 10. Top 6 differentially enriched cell types between saline treated group and normal group. The p-value on each plot was calculated with one-way ANOVA. Also, TukeyHSD as a posthoc analysis was performed to calculate adjusted p-values for each plot. (A) The graph of Tgd cells (one-way ANOVA $P = 0.00012$). (B) The graph of CD4 Tem (one-way ANOVA $P = 0.061$). (C) The graph of Th2 cell (one-way ANOVA $P = 0.017$). (D) The graph of cDC (one-way ANOVA $P = 0.0018$) (E) The graph of fibroblast (one-way ANOVA $P = 0.045$). (F) The graph of pericyte (one-way ANOVA $P = 0.0034$). Tgd: gamma delta T cells, CD4 Tem: CD4 expressing T effector memory cells, cDC: conventional dendritic cell, *: $P < 0.05$, **: $P < 0.01$, ***: $P < 0.001$.

using T_{reg} immunofluorescence images. In the spleen, the ST- H_2S lipo treated group showed a brighter signal compared to the saline treated group ($P < 0.05$; Figure 7G, H). In the colon, both ST- H_2S lipo and LC- H_2S lipo induced to a greater degree more T_{reg} differentiation than that of the saline group ($P < 0.001$ and $P < 0.0001$, respectively) (Figure 7G, H). Lastly, serum markers related to the inflammatory process were compared between the groups (ST- H_2S lipo, LC- H_2S lipo, and saline treated DSS induced colitis model groups and the normal group). While C-reactive protein (CRP), a marker for systemic inflammation, was significantly higher in the saline treated group compared to the normal group ($P < 0.0001$), and only the ST- H_2S lipo treated group showed a significantly lower CRP concentration compared to the saline treated group ($P < 0.05$), indicating its effect in systemic immune modulation. The ST- H_2S lipo treated group tended to have a lower concentration of CRP compared to the LC- H_2S lipo treated group ($P = 0.18$). Moreover, IL-6, TNF- α , and pro-inflammatory cytokines were significantly higher in the saline treated groups ($P < 0.0001$, $P < 0.0001$, respectively), and their concentrations were significantly lower in both the ST- H_2S lipo and LC- H_2S lipo treated groups compared to the saline treated group (IL-6, $P < 0.0001$ and 0.0001 ; TNF- α , $P < 0.001$ and $P < 0.0001$, respectively). The ST- H_2S lipo treated group tended to have a lower concentration of IL-6 compared to the LC- H_2S lipo treated group ($P = 0.18$). Furthermore, IL-4, an anti-inflammatory cytokine, was significantly higher in both the ST- H_2S lipo and LC- H_2S lipo treated groups compared to the saline treated group ($P < 0.01$ and $P < 0.05$, respectively) (Figure S9). Finally, we examined the histology of the major organs after the treatment to assess the potential *in vivo* toxicity of ST- H_2S lipo. There was no overt organ damage in the ST-

H_2S lipo or ST- H_2S lipo treated group (Figure S10). Taken together, we found that 1) ST- H_2S lipo has a superior protective effect compared to unloaded GYY4137, and 2) ST- H_2S lipo showed a higher protective effect compared to LC- H_2S lipo, potentially due to a higher systemic immunomodulatory effect (Figure 8).

Transcriptomics-Level Analysis of Immunomodulatory Process by H_2S lipos in Colitis Model. We explored transcriptomics-level of immunomodulatory processes of ST- H_2S lipo and LC- H_2S lipo in the DSS induced colitis model. RNA-seq data sets of four groups (i.e., normal group, saline, ST- H_2S lipo, and LC- H_2S lipo treated group) were obtained from colonic tissues after treatment of the DSS induced colitis model. We obtained differentially expressed genes (DEGs) between the two groups; saline treated group vs normal group, LC- H_2S lipo treated group vs saline treated group, ST- H_2S lipo treated group vs saline treated group, and LC- H_2S lipo treated group vs ST- H_2S lipo treated group. The volcano plots of DEGs showed the profiles of significantly up-regulated and down-regulated genes between the groups (Figure 9A, Tables S1–S7). Next, the functional annotation of each group was acquired through the gene ontology (GO) analysis (Figure 9B, C and Figure S12). In the saline treated group, the expression of inflammation-related genes (e.g., “cytokine-mediated signaling pathway”) and genes interfered with colon restoration (e.g., “cellular response to interferon-beta”) are increased than normal group, which reflects the active inflammatory process in the DSS induced colitis model.^{32–34} Conversely, the expression of extracellular matrix (ECM) related genes (e.g., “collagen-containing extracellular matrix”) was decreased than normal group, indicating destruction of stromal structure of saline treated group (Figure 9B). In the GO of the LC- H_2S

lipo treated group, the expression of Wnt signaling pathway related genes was increased than that of the saline treated group (Figure S12). The Wnt signaling pathway inhibits the pro-inflammatory NF κ B signaling pathway and is involved in colonic epithelial homeostasis through crypt preservation and tissue regeneration in the colitis model.³⁵ Conversely, the expression of genes related to inflammation (e.g., “cytokine-mediated signaling pathway”) and innate immune response (e.g., “neutrophil chemotaxis”, “granulocyte migration”) was decreased than that of the saline treated group, indicating alleviation of inflammatory process in the LC-H₂S lipo treated group.³⁶ In GO of the ST-H₂S lipo treated group, the expression of genes related to activity of muscle and fiber (e.g., “muscle system process”, “myofibril assembly”) was increased than that of the saline treated group, which could reflect the restoration of the colonic smooth muscle layer in the ST-H₂S lipo treated group (Figure 6C). Conversely, the expression of genes related inflammation (e.g., “response to interferon-gamma”, “response to tumor necrosis factor”) and inhibiting colon restoration (e.g., “response to interferon-beta”) were decreased than that of the saline treated group, also indicating alleviation of the inflammatory process in the ST-H₂S lipo treated group (Figure 9C).

In xCell analysis, the top six differentially enriched cell types between the saline treated group and the normal group were gamma delta T cells (Tgd cell), CD4 expressing T effector memory cells (CD4 Tem), type 2 helper T cells (Th2 cell), conventional DC (cDC), fibroblast, and pericyte. We compared the expression of the six cell types to assess the immunomodulatory effect of ST-H₂S lipo and LC-H₂S lipo (Figure 9C). The Tgd cell showed the highest expression in the saline treated group. The expression of the Tgd cell was reduced in both the ST-H₂S lipo and LC-H₂S lipo treated groups compared to the saline treated group (Figure 10A, $P < 0.001$, $P < 0.001$, respectively). It has been known that large numbers of Tgd cells accumulate in the site of colitis in the DSS induced colitis model.³⁷ The decreased expression of Tgd cells indicates H₂S lipos could inhibit Tgd cell activity in mucosa and alleviate colonic inflammation. The expression of CD4 Tem tended to increase in the saline treated group compared to the normal group ($P = 0.14$). The expression of these cells was not reduced in the LC-H₂S lipo group, but it tended to be reduced in the ST-H₂S lipo treated group compared to the saline treated group (Figure 10B) ($P = 0.117$). As the infiltration of pathogens in the colon increases, CD4 T cells tend to differentiate into CD4 Tem cells.³⁸ The expression of Th2 cells tended to increase in the saline treated group compared to the normal group (Figure 10C) ($P = 0.17$). Interestingly, the expression of these cells was more increased in the LC-H₂S lipo group, but tended to have lower expression in the ST-H₂S lipo treated group compared to the saline treated group ($P = 0.0982$). In addition, the expression of Th2 cells was significantly lower in the ST-H₂S lipo treated group compared to the LC-H₂S lipo group ($P < 0.05$). Ulcerative colitis is characterized by an inflammatory response mediated by Th2 cells rather than Th1 cells. Th2 cells increase the production of pro-inflammatory cytokines (e.g., IL-5, IL-13) and promote the proliferation of T cells and macrophages.^{39,40} The expression of cDC was dramatically reduced in the saline treated group, but the ST-H₂S lipo treated group showed a tendency toward restoration of this cell type (Figure 10D). cDC cells are known to be critical for maintaining immunohomeostasis in the colon. They can induce IFN-1,

which decreases the migration of neutrophils and monocytes to sites of inflammation, leading to the improvement of colonic inflammation.⁴¹ The expression of fibroblasts significantly decreased in the saline treated group compared to the normal group ($P < 0.05$). The expression of pericytes, which regulate endothelial cells, was significantly reduced in the saline and LC-H₂S lipo treated groups compared to the normal group ($P < 0.01$ and $P < 0.01$, respectively). However, the expression of pericytes was not significantly different in the ST-H₂S lipo treated group compared to the normal group ($P = 0.424$), indicating that the vasculature in the colon was successfully restored in the group⁴² (Figure 10E, F).

Among the signaling pathways in PROGENy analysis, androgen, JAK-STAT, NF κ B, and TNF- α were the prominently upregulated pathways in the saline treated group compared to in the normal group ($P < 0.01$, $P < 0.001$, $P < 0.01$, and $P < 0.01$, respectively). Both the inflammatory nuclear factor- κ B (NF κ B) and tumor necrosis factor α (TNF- α) signaling pathways were reduced in the H₂S lipos treated group (Figure S13). Both signaling pathways are known to be inhibited by H₂S.^{43,44} Also, the JAK-STAT signaling pathway was reduced in the H₂S lipos treated group compared to in the saline treated group (ST-H₂S lipo treated group: $P = 0.016$, LC-H₂S lipo treated group: $P = 0.029$). The JAK-STAT signaling pathway is related to multiple pro-inflammatory cytokines.⁸

DSS is a sulfated polysaccharide with various molecular weights, and the DSS induced colitis model has contributed to understanding the pathogenesis of IBD. The mechanism of the DSS induced colitis model has not been clearly identified. However, the considered main cause of pathophysiology is a pathogen invading the mucus membrane damaged by DSS; bacteria and their products.^{45–47} We confirmed that genes related to response bacteria (i.e., response to lipopolysaccharide, response to molecule of bacterial origin) were upregulated in the GO analysis comparing the saline treated group and the normal group (Figure 9B). After oral administration of DSS in mice, an immune response is activated against bacteria infiltrating the damaged colonic tissue, and the immune cell population changes according to the phase of inflammation. Hall et al. reported that a decrease in innate immune cells (i.e., neutrophil) and an increase in adaptive immune cells (i.e., DC, helper T cells, cytotoxic T cells, B cells; immune cells migrating from the spleen) toward the late-acute phase (day 12) of the DSS induced colitis model.⁴⁸ In this study, ST-H₂S lipo and LC-H₂S lipo resulted in different consequences of inflammatory responses in the DSS induced colitis model and showed better therapeutic effects in ST-H₂S lipo. Although the study is needed to illustrate the exact cause of better therapeutic effects of ST-H₂S lipo, migration of splenic immune cells to damaged colonic tissue and transcriptomic-level evidence of immunomodulatory processes may be attributable.

In this study, we developed a simple spleen targeted delivery strategy for H₂S donors using one of the most widely used drug delivery systems, a PEGylated liposome. We identified the ideal PEG size and ratio for a spleen targeting H₂S donor delivering liposome (ST-H₂S lipo) by comparing the stability, drug loading efficiency, *in vitro* H₂S level, and *in vivo* biodistribution. Our ST-H₂S lipo induced M2 phenotypic differentiation *in vitro*, enhanced *in vivo* splenic T_{reg} differentiation in the normal and DSS induced mouse colitis model, and had a pronounced protection effect in the DSS induced

mouse colitis model. Furthermore, ST-H₂S lipo demonstrated an even higher protective effect compared to the H₂S donor loaded conventional long circulating liposome (LC-H₂S lipo) in the DSS induced mouse colitis model, which may be attributed to the higher efficiency of ST-H₂S lipo improving systemic immune homeostasis.

Gasotransmitters are endogenously produced by various enzymes in mammalian cells. NO production is catalyzed from L-arginine by a family of NO synthases (NOSs). CO production is catalyzed by a family of heme oxygenases (HMOXs, also known as HOs) which drives oxidative degradation of heme. H₂S production is catalyzed by CBS, CSE, and MPST (also known as MST).^{11,49,50} Studies have reported the expression of gasotransmitter related enzymes in UC patients and the colitis model. For H₂S related enzymes, their degree of expression is dissimilarly reported. Kyle et al. reported that CSE expression and H₂S synthase are significantly increased in the colitis model (>12-fold and >7-fold, respectively).⁵¹ Additionally, Hirata et al. reported that the expression of CBS and CSE is significantly increased.⁵² These studies suggested that the increased H₂S by up-regulated enzymes promotes ulcer healing and ameliorates inflammation as an anti-inflammatory molecule and not pathogenesis. In contrast, Wallace et al. reported that the expression of CBS and CSE is significantly decreased in severe colonic injury of the colitis model.¹⁸ De et al. reported that the expression of CBS mRNA and protein in the colitis model is significantly down-regulated and H₂S levels decreased.⁵³ In UC patients, Shanwen et al. reported that CBS expression is decreased compared to normal sites.⁵⁴ To sum up, studies have shown that 1) expression of H₂S related enzymes could be increased or decreased, and 2) increased H₂S by up-regulated enzymes drives anti-inflammatory reaction. This evidence could be one of the rationales to use H₂S donor therapeutics in UC. In CO related enzymes, HMOX-1 has been mainly studied. In UC patients, HMOX-1 expression was heterogeneous according to severity. HMOX-1 expression is increased at the site of a mild inflammatory reaction. On the other hand, HMOX-1 expression is decreased at the site of a severe inflammatory reaction.⁵⁵ These results may explain our observation using transcriptomics data that showed an increased expression of HMOX-1 in the colitis model but decreased the expression in patients with UC. Because CO is decreased in severe UC, it could be a therapeutic material as well. Recently, it has been reported that CO delivery by gas-entrapping materials induced a therapeutic effect in the DSS induced colitis mouse model.⁵⁶ NO has long been known to be involved in inflammatory reactions in UC. NO especially leads to tissue injury by oxidative metabolism and is produced in activated macrophages and neutrophils. Additionally, the NOS activity in UC patients was 10-fold higher than in the normal group,^{57,58} which is a similar finding with our transcriptomics data analysis in the colitis model and patients with UC.

H₂S has anti-inflammatory activity in cardiovascular, respiratory, and gastrointestinal systems in various pathological conditions.^{59–61} Particularly, in gastrointestinal systems, the effects of H₂S in immune modulation are well reported in various pathological conditions. Induction of a stomach ulcer in a rat resulted in an increased endogenous H₂S level, and an inhibitor of endogenous H₂S reduced the ulcer healing process.¹⁹ In the colitis model, H₂S donors showed notable therapeutic effects. Inhibiting the endogenous synthesis of H₂S resulted in severe mucosal injury and inflammation of the

colon. In contrast, H₂S donors significantly reduced the colitis severity and proinflammatory tumor necrosis factor (TNF)- α cytokine.¹⁸ Furthermore, delivering H₂S into the colon helps to restore the microbiota biofilm and increases the mucus granules.¹⁷ H₂S can induce immune cell differentiation into an anti-inflammatory form, resulting in an anti-inflammatory effect. For example, H₂S induced M2 macrophage polarization, resulting in amelioration of myocardial infarction-induced cardiac functional deterioration.²⁸ Moreover, H₂S is required for T_{reg} cell differentiation and immune homeostasis via forkhead box (FOXP3) demethylation, and H₂S deficiency led to an autoimmune disease.⁶² Specifically, H₂S promotes the expression of ten-11 translocation protein (TET1) and TET2 to maintain the demethylation of forkhead box P3 (FOXP3).^{62,63} Meanwhile, T_{reg} has an important role in the pathogenesis of IBD.⁵ In T_{reg} depleted mice, inflammatory cytokine and aggravated inflammation of the intestine were increased. In addition, T_{reg} cells are responsible for inhibiting the interaction between T cells and antigen presenting cells (APCs).^{28,62,64} Additionally, IBD patients showed apoptosis of T_{reg} at the inflammation site of the colon.^{65–68} Therefore, we selected T_{reg} differentiation as a key immune modulation marker to assess the protective effect of the ST-H₂S lipo in the DSS induced colitis model in this study.

Structurally, the spleen consists of red pulp (RP), white pulp (WP), and marginal zone (MZ). The spleen is a reservoir of various immune cells. In the RP, monocytes, macrophages, and dendritic cells are abundant. The primary role of the RP is to filter blood borne pathogens and damaged erythrocytes. WP consists of B cells, T cells, and dendritic cells, which are responsible for antigen specific immune responses to viral, bacterial, and fungal infections.⁶⁹ Macrophages and metallophilic macrophages, B cells, and dendritic cells are located in the MZ. Marginal zone macrophages can internalize blood borne pathogens and damaged molecules.⁷⁰ Moreover, in the MZ, APCs ingest antigens and migrate into the WP for interaction with lymphocytes. The interaction between the lymphocytes of the WP and APCs could induce T_{reg} cell differentiation from naive T cells.^{24,71} The spleen has a crucial role in regulating immunological responses in various pathological states such as ischemic stroke,⁷² myocardial infarction⁷³ and infections including coronavirus disease 2019 (COVID-19).^{24,74} The progression of these pathological conditions is strongly associated with the regulation of immune cells in the spleen. For example, in ischemic myocardial injury, monocytes in the spleen are mobilized and recruited to the ischemic myocardium. The recruited monocytes have critical roles in the regulation of inflammation and repair of damaged tissue.⁷⁵ Therefore, spleen mediated immune modulation is gaining momentum as a therapeutic target in various pathologic conditions related to unregulated inflammation.^{23,76,77}

The liver and spleen have a natural characteristic to clear nanoparticles from systemic circulation because they are a natural filter for blood borne pathogens and antigens which can have a similar size with nanoparticles. This characteristic can reduce the drug delivery efficiency to diseased tissue such as tumors or inflammatory lesions. Therefore, long circulating nanoparticles have been developed to reduce and delay nanoparticle uptake in the liver and spleen. However, recently, studies on the redirection of nanoparticles to target the spleen are gaining attention for immune modulative therapy.⁷⁸ In an experiment on polystyrene nanoparticle biodistribution during

Table 1. Therapeutic Potential of Various Spleen Targeting Nanoparticles^a

| Type of disease model | Nanoparticles | Size (nm) | Zeta potential (mV) | Stealth polymer | Spleen targeting strategy | Spleen targeting efficiency (%) ^a | Ref |
|-----------------------|--------------------------|---------------|---------------------|--------------------------|---|--|------------|
| Tumor | iPSC@RBC-Mlipo | 184 | 4.7 | DSPE-PEG ₂₀₀₀ | Damaged erythrocyte membrane entrapped by spleen | 190 | 23 |
| Tumor | Ag encapsulated PL | Not mentioned | Not mentioned | DSPE-PEG ₂₀₀₀ | Repeated preinjection of empty PL for delivering Ag encapsulated PL to splenic marginal zone B cell | N/A | 82 |
| Leishmaniasis | AmB loaded SCNPs | 333 ± 7 | -13.9 ± 0.24 | N/A | Targeting resident macrophage | 50.9 | 83 |
| Rheumatoid arthritis | Actarit loaded SLNs | 241 ± 23 | -17.14 ± 1.6 | N/A | Passive targeting to RES organs | 120 | 84 |
| Atherosclerosis | PS | 113.7 | -0.2 ± 1.68 | PEG-bl-PPS | Changing the nanostructure morphology | 16.7 | 85 |
| Tumor | RNA-LPX | 200–320 | Around -30 | N/A | Negative charged lipid nanocarrier | N/A | 86 |
| IBD | ST-H ₂ S lipo | 110.3 ± 42.4 | -28.1 | DSPE-PEG ₅₀₀₀ | Ideal PEG size and ratio for spleen targeting | 179.9 | This study |

^aSpleen targeting efficiency (%) is calculated by the (spleen uptake of the nanoparticle/the liver uptake of the nanoparticle) × 100. N/A: not applicable, iPSCs: induced pluripotent stem cells, iPSC@RBC-Mlipo: iPSCs encapsulated in coalescent erythrocyte-liposome, PL: PEGylated liposome, iPSC@Mlipo: iPSC encapsulated in liposome, DSPE: 1,2-distearoyl-*sn*-glycero-3-phosphoethanolamine, PEG: polyethylene glycol, AmB: amphotericin B, SCNPs: 4-sulfated *N*-acetyl galactosamine conjugated chitosan nanoparticles, SLN: solid lipid nanoparticle, TEC: overall targeting efficiency, PS: polymersome, PEG-bl-PPS: poly(ethylene glycol)-*bl*-poly(propylene sulfide), RNA-LPX: RNA-lipoplexes, DCs: dendritic cells, IBD: inflammatory bowel disease.

systemic inflammation, nanoparticles with a 20, 100, and 500 nm size mostly accumulated in the marginal zone of the spleen. Particularly, the nanoparticles were more dramatically accumulated in the spleen when inflammation was induced in mice by lipopolysaccharide.^{79,80} Conventionally, one of the most effective strategies for a longer circulation was to modify the nanoparticle surface using polyethylene glycol (PEG). PEG helps nanoparticles to maintain a more stable condition, evade the immune system, and enhance the delivery efficacy to the target region.⁸¹ Considering spleen targeting, surface PEG does not appear to be an appropriate component of nanoparticles. Therefore, we tested various sizes and ratios of PEG to achieve a high stability, drug loading efficiency, and effective spleen targeting. Many studies have reported on the therapeutic potential of spleen targeting by various approaches. In a treatment study on experimental autoimmune encephalomyelitis (EAE), antigens linked to syngeneic splenic leukocytes with ethylene carbodiimide (Ag-SP) accumulated in the MZ. Consequently, they induced T_{reg} differentiation.⁷⁶ In a treatment study using an inflammatory arthritis model, noninvasive ultrasound stimulation into the spleen showed a reduction of the disease severity through the cholinergic anti-inflammatory pathway.⁷⁷ Especially, many studies have reported on the therapeutic potential of spleen targeting nanoparticles (Table 1). Zhai et al. developed induced pluripotent stem cells (iPSCs) encapsulated in coalescent erythrocyte-liposome (iPSC@RBC-Mlipo). As mentioned above, the spleen has the ability to filter damaged erythrocytes. iPSC@RBC-Mlipo used the characteristic of spleen targeting. In terms of the spleen targeting efficiency, iPSC@RBC-Mlipo was three times higher compared to iPSC encapsulated in liposomes (iPSC@Mlipo). In the treatment of the B16F10 tumor model, iPSC@RBC-Mlipo showed a significantly better antitumor effect and inhibition of metastasis than that of iPSC@Mlipo.²³ Shimizu et al. developed an antigen (Ag) encapsulated PEGylated liposome (PL). As a spleen targeting strategy, the phenomenon when more PL is repeatedly administered, more of it accumulates in the splenic MZ, was used. In the treatment of the EG7-OVA tumor model, the group with preinjected empty PL prior to Ag encapsulated PL

injection induced a more obvious cytotoxic T lymphocyte (CTL) immune response and suppressed tumor growth than the group without preinjected empty PL.⁸² Tripathi et al. developed 4-sulfated *N*-acetyl galactosamine which could specifically target resident macrophages in the liver and spleen conjugated chitosan nanoparticles (SCNPs). In the treatment of leishmaniasis, amphotericin B (AmB) loaded SCNPs (AmB-SCNPs) delivered significantly more AmB to the spleen compared to the AmB-chitosan nanoparticles (AmB-CNPs) ($P < 0.05$). Moreover, AmB-SCNPs showed significantly more antileishmanial activity than that of the AmB-CNPs ($P < 0.05$).⁸³ Ye et al. developed a passively spleen targeted actarit, antirheumatic drug, loaded solid lipid nanoparticle (SLN). The actarit-SLN was more accumulated in the spleen than that of the unloaded actarit (6.31% to 16.29%).⁸⁴ Yi et al. studied nanostructure morphology suitable for targeting DCs. Among the nanostructures which were all assembled from poly(ethylene glycol)-*bl*-poly(propylene sulfide) (PEG-bl-PPS), polymersomes (PS) structurally similar to liposomes showed the highest uptake in the splenic DCs of normal mice. Interestingly, in the spleen of atherosclerotic Ldlr^{-/-} mice, PS uptake by macrophages was significantly reduced ($P < 0.005$), while PS uptake by DCs was barely changed compared to that by normal mice. As a result, PS was predominantly phagocytosed by splenic DCs compared to macrophages in atherosclerotic Ldlr^{-/-} mice ($P = 0.006$).⁸⁵ Kranz et al. developed RNA-lipoplex (RNA-LPX) with a net charge suitable for DCs targeting. They found that RNA-LPX with about -30 mV was more accumulated in the spleen compared to the positively charged RNA-LPX. In the treatment of several tumor models, the selected RNA-LPX formulation for delivering RNA to the spleen induced strong immune responses and showed an antitumor efficacy due to systemic DC targeting.⁸⁶ In the present study, we developed a simple spleen targeting strategy by modulating the PEG type and ratio, in arguably the most frequently used nanoparticles for drug delivery, a PEGylated liposome. When comparing the spleen targeting efficiency (%), ST-H₂S lipo was one of the best targeting nanoparticles among the reported spleen targeting nanoparticles.^{23,83–85} We found

the ideal composition of PEG to obtain a reasonable loading efficiency, stability and excellent spleen targeting ability.

CONCLUSIONS

In conclusion, we developed spleen targeting H₂S donor loaded liposomes (ST-H₂S lipo). Our ST-H₂S lipo demonstrated an excellent loading capacity of H₂S donor and stability. Additionally, ST-H₂S lipo induced a M2 phenotypic change in macrophages after efficient cell uptake and H₂S release in the *in vitro* experiments. The excellent spleen targeting ability of the ST-H₂S lipo was confirmed by PET and IVIS imaging. In the treatment of the DSS induced colitis model, we found that ST-H₂S lipo showed a significantly greater therapeutic effect than that of the unloaded H₂S donor. Moreover, ST-H₂S lipo demonstrated an even higher protective effect compared to the H₂S donor loaded conventional long-circulating liposome (LC-H₂S lipo). ST-H₂S lipo treatment showed a higher systemic immune modulative effect compared to the LC-H₂S lipo treatment. These findings demonstrate the potential of the spleen targeting H₂S lipo in the treatment of IBD.

EXPERIMENTAL SECTION

Synthesis of H₂S lipo. The self-assembled H₂S lipo comprised DSPC, cholesterol, GYY4137, and DSPE-PEG (Figure 2A). GYY4137 has been studied in diverse fields.^{60,87,88} All experimental groups comprised identical mass ratios of DSPC and cholesterol (6:1). First, 133.3 μM H₂S donor was prepared for H₂S lipo. Additionally, 600 μM H₂S donor was prepared for reducing the administration volume of DSS treatment. The composition of H₂S lipo was dissolved in organic solvent chloroform/methanol (3:1 v/v) and evaporated. Dried lipids were vacuumed overnight for removing the residual organic solvent. Dried lipids formed bilamellar vesicles through adding distilled water (DW) at 37 °C. Then, H₂S lipo was formed with several cycles of ultrasonication. In the end, H₂S lipo was filtered using a 0.2 μm filter and size exclusion chromatography.

Detection of H₂S Release from H₂S lipo. H₂S released by H₂S donor or H₂S lipo was identified by a precipitation reaction with silver nitrate (AgNO₃).²⁷ First, AgNO₃ was added to a solution including H₂S donor or H₂S lipo. DW with H₂S lipo was added to methanol to destroy the liposomal structure. Released H₂S reacted with AgNO₃, and then the product, silver sulfide (Ag₂S), was sedimented. Ag₂S was detected through a colorimetric assay. The OD of Ag₂S was 405 nm. The H₂S donor and H₂S lipo were quantitatively calculated by a standard curve. When doing the colorimetric assay, we added reagent, AgNO₃, and methanol in a 1:1:3 ratio.

Size Stability and Loading Efficiency of H₂S lipos. The stability of H₂S lipos was investigated using size distribution profiles. The investigated H₂S lipo was suspended with DW and stored at room temperature. Size distribution profiles were acquired by DLS. The acquisition time points were day 0, 3, 7, and 14. For reflecting stability under physiological conditions, H₂S lipo was suspended with 50% FBS in PBS and stored at 4 °C. The acquisition time points were day 0, 1, 2, 3, 4, 5, and 6. Loading efficiency of H₂S lipos was compared by a colorimetric assay at 90 min after the precipitation reaction. Serial concentration groups of GYY4137 were simultaneously performed for calculating the standard curve. The measured OD value is converted into molar concentration using indicated GYY4137 molecular weight and the standard curve. The loading efficiency (%) of H₂S lipo was calculated using the following formula: loading efficiency (%) = GYY4137 mass converted from measured OD/initial GYY4137 mass × 100%.

In Vitro Experiments Using H₂S lipo. The macrophage cell line, RAW 264.7, was used for *in vitro* experiments. 10⁵ cells were incubated in a confocal dish. The next day, saline, GYY 4137, and fluorescent H₂S lipo were treated in RAW 264 cells, respectively. Fluorescent H₂S lipo was used for examining cell uptake of H₂S lipo. The FITC was mixed with DSPE-PEG2k-Amine in the same

molecular weight. The mixture was dissolved in an organic solvent when H₂S lipo was synthesized. The time points of cell uptake images were 0, 1, 2, and 3 h. The fluorescence intensity was quantified using ImageJ. In the cell differentiation study, we assessed the ability of promoting anti-inflammatory (M2) macrophage differentiation. The 64.57 μM GYY 4137 and H₂S lipo were treated in RAW 264.7 cells. We observed elongated RAW 264.7 cells after 48 h. The elongation factor (AU) was used as an assessment method of macrophage differentiation.⁴⁵ The elongation factor is the number of dividing longitudinal cell length into cross-sectional cell length. It indicated through M2 macrophage differentiation that the elongation factor increased. Saline, bare lipo, GYY 4137, and H₂S lipo are used as the reagents, respectively. All images were acquired with a confocal scanning microscope.

The Comparison of In Vitro H₂S Release between Various PEGylation Strategies of H₂S lipo. In the H₂S release test, 10⁵ cells of RAW 264.7 were incubated in a confocal dish. The next day, cells were treated with reagents. The reagents were saline, GYY 4137, and H₂S lipos. Various PEGylation strategies of H₂S lipo were used for comparing the H₂S release ability depending on the mass ratio of DSPC/DSPE-PEG and the type of PEG. After 2 h from treating the reagents, a H₂S detection probe, Hsp-1, was used to identify released H₂S.⁸⁹ The fluorescence intensity of released H₂S was quantified using ImageJ. All images were acquired with a confocal scanning microscope.

The Cell Viability Assessment after Treating H₂S lipo. The RAW 264.7 cell line was treated with H₂S lipo in medium (DMEM with 5% FBS). H₂S lipo was serially diluted based on molar concentration. After 24 h treatment with H₂S lipo, 0.5 mg/mL of 3-[4,5-dimethylthiazol-2-yl]-2,5-diphenyltetrazolium bromide reagent (MTT) was added, and the solution was incubated at 37 °C for 3 h. After removal of the reagent, 100 μL of DMSO was added. Absorbance at 540 nm was detected with a microplate spectrophotometer.⁹⁰

Radiolabeling Method of H₂S lipo. The composite structure made of a chelator and PEG was used to synthesize radiolabeled H₂S lipo. First, 2-(*p*-isothiocyanatobenzyl)-1,4,7-triazacyclononane-*N,N',N'*-triacetic acid trihydrochloride ((*p*-SCN-Bn)-NOTA) as a chelator and PEG-amine were dissolved in methanol with the same molar ratio. *N,N*-Diisopropylethylamine (DIPEA) was added in the mixture for inducing the covalent bond. The mixture was allowed to react overnight. Then, a PEG conjugated chelator was added in H₂S lipo synthesis before the evaporating process. The chelated H₂S lipo was mixed with a radioisotope in a pH 5 solution adjusted by 2 M sodium acetate. The final mixture was incubated at 37 °C for 30 min. In the end, serial size exclusion chromatography was conducted for sorting purified radiolabeled H₂S lipo. The radiolabeling efficiency was assessed by radio-thin layer chromatography (TLC) which is iTLC plates with a 50 mM EDTA solution.

In Vivo PET Images of Radiolabeled H₂S lipo. The compared compositions were H₂S lipo_{5k-2}, H₂S lipo_{5k-6} and H₂S lipo_{5k-12}. Here 50 μCi of ⁶⁴Cu radiolabeled H₂S lipo (⁶⁴Cu-H₂S lipo) in saline was injected into a normal C57/BL6N mouse intravenously. The chronological PET Images were acquired by a PET scanner (GENESYS4). The acquisition time points of the PET images were 0, 2, 12, and 36 h. A quantitative analysis was conducted by MIM Encore (MIM software Inc., OH, USA). The calculated region of interest (ROI) was blood pool, spleen, liver, and muscle. The time-activity curve of bloodpool was calculated by a fit curve equation. The ROI was quantified as the percentage of the injected dose per tissue weight (%ID/g). The standard uptake value (SUV) was calculated by the following formula: (tissue radioactivity concentration)/[(injected dose)/(bodyweight)]. A time-activity curve was calculated by fitting equation ($y = y_0 + a \times e^{-bx}$) using the SUV_{mean} of bloodpool at 0, 2, 12, and 36 h.

In Vivo Biodistribution of Fluorescent H₂S lipo in DSS Induced Colitis Model. Fluorescent H₂S lipo was used to compare the biodistributions between ST-H₂S lipo and LC-H₂S lipo in the DSS induced colitis model. A fluorescence dye, 1,1'-dioctadecyl-3,3,3',3'-tetramethylindotricarbocyanine iodide (DiR), was dissolved

in an organic solvent with the H₂S lipo composite before the evaporating phase. The 8-week-old C57/BL6 mice were the induced colitis model using DSS. The reagents were intravenously injected into colitis model mice at 7 days from giving DSS. The next day, injected mice were sacrificed and dissected for organs. The collected organs were heart, muscle, lung, kidney, liver, spleen, small intestine, and colon. Fluorescence images of the organs were acquired by an IVIS instrument. All fluorescence images of organs were quantified using living image 2.5.

Comparison of H&E-Stained Images and Fluorescent Images. It is widely accepted that hematoxylin and eosin (H&E) staining can exhibit histological characteristics in diverse tissues such as lymphoma, breast cancer, and prostate cancer. When identifying spatial clusters from H&E-stained images, various clustering algorithms, including the K-means algorithm, Watershed algorithm, and the Otsu thresholding method, have been proposed. Among them, K-means algorithm is the most popular. Spleen tissues are especially characterized by the structure of RP, WP, and the MZ, so it is expected that identification of these histological structures through clustering algorithms can be easily performed. K-means clustering was used according to the literature.⁹¹ After defining a patch of 32 × 32 size around each pixel in a H&E staining image, 512 features were extracted for each patch by using the VGG16 pretrained CNN model. After that, K-means clustering was applied to cluster pixels in the image. K was set as 5 to represent background, border of each tissue, RP, MZ, and WP, and then the border of each tissue was also indicated as the background. Lastly, each defined section of the H&E image was compared with the corresponding fluorescence image to quantify the amount of fluorescence in each histological region.

Transcriptomics-Level Analysis of Gasotransmitters. The RNA expression profiles of UC patients (GSE38713) and the DSS induced colitis model (GSE31906) were derived from the gene expression omnibus (GEO) of the National Center for Biotechnology Information. Investigated RNA expression of gasotransmitter related enzymes were cystathionine-beta-synthase (CBS), cystathionine-gamma-lyase (CTH), 3-mecaptopyrivate sulfurtransferase (MPST), nitric oxide synthase 1 (NOS1), nitric oxide synthase 2 (NOS2), heme Oxygenase 1 (HMOX1), and heme oxygenase 2 (HMOX2). The CBS, CTH, and MPST released H₂S. NOS1 and 2 released NO. HMOX1 and 2 released CO. In GSE38713, the rectum or sigmoid colon was extracted from UC patients ($n = 23$) and the control group ($n = 20$) for RNA expression analysis. Subjects which were diagnosed at least 6 months before were selected as UC patients. Subjects which had no lesion or mild symptoms in gastrointestinal tracts were selected as the control group. In GSE31906, the distal colon (about 8 cm) was extracted from the colitis model ($n = 27$) and the control group ($n = 9$). The raw data of GSE38713 and GSE31906 was analyzed using Bioconductor tool of R software (Pardeck Inc., MO, USA).^{92,93}

Animals and DSS Induced Colitis Model. The C57BL/6 female mice were purchased from the Institute for Experimental Animals, College of Medicine, Seoul National University. All experimental protocols were screened and approved by the Institutional Animal Care and Use Committee of Seoul National University. All mice were housed in a specific pathogen free (SPF) facility. The colitis model was induced by 3% DSS (36–50 kDa). The mice received 3% DSS water for 7 days. Then normal drinking water was given for 5 days.

DSS Induced Colitis Model Treatment. The 8-week-old C57/BL6 female mice were induced for colitis model using DSS. Tap water with 3% DSS was given except for the normal group.⁹⁴ 3% DSS water was given up to 7 days in the study for comparing groups which were normal, saline, GYY 4137 (60 μM and 100 μM), and ST-H₂S lipo (60 μM and 100 μM).⁹⁵ In a comparison test between ST-H₂S lipo and LC-H₂S lipo, 3% DSS water was given up to 6 days in the study. The reagents were intravenously injected every day (Figure 6A) or every other day (Figure 7A). The weight change (%) was daily recorded for checking disease conditions. The colitis models were sacrificed using a CO₂ chamber. The spleen and colon were extracted. The red blood cell (RBC) lysis buffer was used when the spleen was extracted. The

whole colon length was examined for comparing contraction by inflammation. The distal 3 cm of colon samples was used to colon weight and H&E staining. The colon per length was examined for granular immune cell accumulation. The histological analysis was conducted using H&E images of the colon. The method of inflammation score was performed according to refs 63 and 96. The score is marked by 0 to 11. The categories of inflammation score are severity of inflammation (1 to 4), extent of inflammation (1 to 3), presence of epithelial hyperplasia (0 or 1), and presence of ulceration (0 or 3).

RNA-Seq Analysis. Twelve C57BL/6N mice were prepared for bulk RNA sequencing (bulk RNA-seq) analysis. Four groups of three mice were then defined as follows: an untreated group, normal; a DSS-treated group, saline treated group, ST-H₂S lipo treated group, LC-H₂S lipo treated group. The bulk RNA-seq data sets for four groups were then obtained via QuantSeq 3'mRNA-seq (Illumina) ($n = 3$, respectively). Excel-based DEG Analysis (ExDEGA, version 4.0.3) was performed to calculate normalized expressions, fold changes (FCs), and p-values from bulk RNA-seq data. Here, mouse genes were annotated with a reference of "mm10" (UCSC), and count data was normalized through TMM and CPM. Genes were defined as differentially expressed genes (DEGs) only when the log₂ fold change was greater than 1.5 or less than -1.5 and the p-value was less than 0.05. DEGs among a total of 23,282 genes in each pair of groups with a fold change threshold of 1.5 and a p-value threshold of 0.05 were visualized by EnhancedVolcano (version 1.16.0) in R. The top 100 or all (<100) DEGs with the largest (lowest) FCs were then selected for gene ontology (GO) analysis for up-regulated (down-regulated) DEGs. Dot plots for GO analysis were presented in five categories according to biological process (BP), cellular component (CC), and molecular function (MF). In addition, the top six cell types with the lowest p-value (one-way ANOVA test) for Saline versus Normal among a total of 67 cell types were shown by xCell analysis.⁹⁷ In the analysis, mouse genes were converted into human genes using a conversion table because xCell analysis is one of human-centered bulk RNA-seq deconvolution algorithms. The enrichment of the same cell types was also investigated for LC-H₂S lipo and ST-H₂S lipo. To identify the activity of signaling pathways, PROGENy was introduced. This analysis can estimate the responsiveness of 14 well-known signaling pathways using published perturbation data. When the PROGENy analysis was executed, the top 1,000 genes with the lowest p-values were utilized to generate the model matrix. The whole process was performed in R (version 4.2.2).

Immunofluorescence. The extracted spleen and distal colon were stored in a 4% paraformaldehyde solution. After paraffin blocking, the paraffins were sectioned to 4 μm thickness. The sectioned slices were processed by several phases for immunofluorescence. The xylene was used to remove paraffins in tissue, and then ethanol with serial concentration was used to remove the xylene in tissue. The distilled water was used between each procedure. For antigen retrieval, sectioned tissue was incubated with 0.1% of trypsin for 25 min at 37 °C. Then 0.1% of Triton X-100 was used for permeabilization for 10 min. The 10% FBS was used for blocking. After the procedure of antibody incubation overnight at 4 °C, Hoechst 33342 was used to stain nuclei for 10 min. All images were acquired using a confocal scanning microscope.

Flow Cytometry. Flow cytometry was conducted for assessing immune cell differentiation in the spleen and bone marrow. FOXP3⁺ and CD4⁺ antibodies were used for T_{reg} markers. CD80⁺ and CD206⁺ antibodies were used for M1 and M2 macrophages, respectively. The scheme of gating strategy is illustrated (Figure S6). The extracted spleen and bone marrow were homogenized. The PBS washing was performed between each procedure. All data was acquired with a flow cytometer. All data was analyzed with the Guava Incyte program.

Statistical Analyses. The statistics were performed using GraphPad Prim 8 statistical analysis. Student's *t* tests or Mann–Whitney tests were used to compare RNA expression differences from GEO data. One-way analysis of variance (ANOVA) with a Tukey posthoc test was used to compare three or more groups. The differences with $P < 0.05$ were considered significant.

ASSOCIATED CONTENT

Supporting Information

The Supporting Information is available free of charge at <https://pubs.acs.org/doi/10.1021/acsnano.2c08898>.

Supporting figures, materials, stability test of H₂S lipos, H₂S detection method, radiochemical stability, and various experiments showing that H₂S lipo is an efficient immunomodulator (PDF)

AUTHOR INFORMATION

Corresponding Author

Hyung-Jun Im – Department of Applied Bioengineering, Graduate School of Convergence Science and Technology, Seoul National University, Seoul 08826, Republic of Korea; Department of Molecular Medicine and Biopharmaceutical Sciences, Graduate School of Convergence Science and Technology and Cancer Research Institute, Seoul National University, Seoul 03080, Republic of Korea; Research Institute for Convergence Science, Seoul National University, Seoul 08826, Republic of Korea; orcid.org/0000-0002-4368-6685; Phone: 031-888-9187; Email: iihjij@gmail.com; <http://tmtl.snu.ac.kr>

Authors

Chiwoo Oh – Department of Applied Bioengineering, Graduate School of Convergence Science and Technology, Seoul National University, Seoul 08826, Republic of Korea
Wooseung Lee – Department of Applied Bioengineering, Graduate School of Convergence Science and Technology, Seoul National University, Seoul 08826, Republic of Korea
Jeongbin Park – Department of Molecular Medicine and Biopharmaceutical Sciences, Graduate School of Convergence Science and Technology, Seoul National University, Seoul 03080, Republic of Korea
Jinyeong Choi – Department of Applied Bioengineering, Graduate School of Convergence Science and Technology, Seoul National University, Seoul 08826, Republic of Korea
Somin Lee – Department of Molecular Medicine and Biopharmaceutical Sciences, Graduate School of Convergence Science and Technology, Seoul National University, Seoul 03080, Republic of Korea
Shengjun Li – Department of Molecular Medicine and Biopharmaceutical Sciences, Graduate School of Convergence Science and Technology, Seoul National University, Seoul 03080, Republic of Korea
Han Na Jung – Department of Applied Bioengineering, Graduate School of Convergence Science and Technology, Seoul National University, Seoul 08826, Republic of Korea
Jeong-Seob Lee – Department of Applied Bioengineering, Graduate School of Convergence Science and Technology, Seoul National University, Seoul 08826, Republic of Korea
Jee-Eun Hwang – Department of Molecular Medicine and Biopharmaceutical Sciences, Graduate School of Convergence Science and Technology, Seoul National University, Seoul 03080, Republic of Korea
Jiwoo Park – Department of Molecular Medicine and Biopharmaceutical Sciences, Graduate School of Convergence Science and Technology, Seoul National University, Seoul 03080, Republic of Korea
MinKyu Kim – Department of Applied Bioengineering, Graduate School of Convergence Science and Technology, Seoul National University, Seoul 08826, Republic of Korea

Seungki Baek – Department of Applied Bioengineering, Graduate School of Convergence Science and Technology, Seoul National University, Seoul 08826, Republic of Korea

Complete contact information is available at: <https://pubs.acs.org/doi/10.1021/acsnano.2c08898>

Author Contributions

C.O. proposed concept of idea, performed all studies of the article, and wrote the paper. H.I. designed and directed the research, analyzed the data, and revised the paper. W.L. first synthesized H₂S lipo and designed H₂S detection method using AgNO₃ precipitation. J.P. performed quant-seq analysis for analyzing transcriptomics-level of immunomodulation by H₂S lipos. J.C., S.B., S.L., performed treatment study of DSS induced colitis model. They collected, weighed, and analyzed the organs. H.J., J.L., J.H., J.P., and M.K. participated in laboratory meeting and advised study designs.

Funding

This research was supported by grants funded by the National Research Foundation of Korea (NRF) (NRF-2019M2D2A1A01058210, NRF-2020R1C1C1009000, NRF-2021M2E8A1039564, NRF-2022R1A6A1A03063039), Korea Evaluation Institute of Industrial Technology (KEIT) grant funded by the Korea government (MOTIE) (No. 20018522), and Korea Drug Development Fund funded by Ministry of Science and ICT, Ministry of Trade, Industry, and Energy, and Ministry of Health and Welfare (HN22C0632). Schematic illustrations were created with BioRender.

Notes

The authors declare no competing financial interest.

ACKNOWLEDGMENTS

We are grateful to the Department of Nuclear Medicine at Seoul National University College of Medicine for their assistance with the radioisotope labeling facility and to the Division of RI application at the Korea Institute of Radiological and Medical Sciences (KIRAMS, Seoul, Korea) for supplying us with the ⁶⁴Cu radioisotopes.

REFERENCES

- (1) Kobayashi, T.; Siegmund, B.; Le Berre, C.; Wei, S. C.; Ferrante, M.; Shen, B.; Bernstein, C. N.; Danese, S.; Peyrin-Biroulet, L.; Hibi, T. Ulcerative Colitis. *Nat. Rev. Dis. Primers* **2020**, *6*, 73.
- (2) Abraham, C.; Cho, J. H. Inflammatory Bowel Disease. *N Engl J. Med.* **2009**, *361*, 2066–2078.
- (3) Alatab, S.; Sepanlou, S. G.; Ikuta, K.; Vahedi, H.; Bisignano, C.; Safiri, S.; Sadeghi, A.; Nixon, M. R.; Abdoli, A.; Abolhassani, H.; Alipour, V.; Almasi-Hashiani, A.; Anushiravani, A.; Arabloo, J.; Atique, S.; Awasthi, A.; Badawi, A.; Baig, A. A. A.; Bhala, N.; et al. The Global, Regional, and National Burden of Inflammatory Bowel Disease in 195 Countries and Territories, 1990–2017: A Systematic Analysis for the Global Burden of Disease Study 2017. *Lancet Gastroenterol Hepatol* **2020**, *5*, 17–30.
- (4) Hindryckx, P.; Jairath, V.; D'Haens, G. Acute Severe Ulcerative Colitis: From Pathophysiology to Clinical Management. *Nat. Rev. Gastroenterol Hepatol* **2016**, *13*, 654–664.
- (5) Chang, J. T. Pathophysiology of Inflammatory Bowel Diseases. *N Engl J. Med.* **2020**, *383*, 2652–2664.
- (6) Feuerstein, J. D.; Isaacs, K. L.; Schneider, Y.; Siddique, S. M.; Falck-Ytter, Y.; Singh, S.; Committee, A. G. A. I. C. G.; et al. AGA Clinical Practice Guidelines on the Management of Moderate to Severe Ulcerative Colitis. *Gastroenterology* **2020**, *158*, 1450–1461.
- (7) Jeuring, S. F. G.; Bours, P. H. A.; Zeegers, M. P.; Ambergen, T. W.; van den Heuvel, T. R. A.; Romberg-Camps, M. J. L.; van

- Bodegraven, A. A.; Oostenbrug, L. E.; Breukink, S. O.; Stassen, L. P. S.; Hameeteman, W. H.; Masclee, A. A. M.; Jonkers, D. M. A. E.; Pierik, M. J. Disease Outcome of Ulcerative Colitis in an Era of Changing Treatment Strategies: Results from the Dutch Population-Based Ibdsl Cohort. *J. Crohn's Colitis* **2015**, *9*, 837–845.
- (8) Salas, A.; Hernandez-Rocha, C.; Duijvestein, M.; Faubion, W.; McGovern, D.; Vermeire, S.; Vetrano, S.; Vande Castele, N. Jak-Stat Pathway Targeting for the Treatment of Inflammatory Bowel Disease. *Nat. Rev. Gastroenterol Hepatol* **2020**, *17*, 323–337.
- (9) Kucharzik, T.; Maaser, C. Infections and Chronic Inflammatory Bowel Disease. *Visceral Medicine* **2014**, *30*, 326–332.
- (10) Baumgart, D. C.; Le Berre, C. Newer Biologic and Small-Molecule Therapies for Inflammatory Bowel Disease. *N Engl J. Med.* **2021**, *385*, 1302–1315.
- (11) Mustafa, A. K.; Gadalla, M. M.; Snyder, S. H. Signaling by Gasotransmitters. *Sci. Signal* **2009**, *2*, re2.
- (12) Szabó, C. Hydrogen Sulphide and Its Therapeutic Potential. *Nat. Rev. Drug Discovery* **2007**, *6*, 917–935.
- (13) Zhao, W.; Ndisang, J. F.; Wang, R. Modulation of Endogenous Production of H₂S in Rat Tissues. *Can. J. Physiol. Pharmacol.* **2003**, *81*, 848–853.
- (14) Wang, Y.; Zhao, X.; Jin, H.; Wei, H.; Li, W.; Bu, D.; Tang, X.; Ren, Y.; Tang, C.; Du, J. Role of Hydrogen Sulfide in the Development of Atherosclerotic Lesions in Apolipoprotein. *E Knockout Mice* **2009**, *29*, 173–179.
- (15) Szabo, C. Roles of Hydrogen Sulfide in the Pathogenesis of Diabetes Mellitus and Its Complications. *Antioxid Redox Signal* **2012**, *17*, 68–80.
- (16) Fiorucci, S.; Antonelli, E.; Distrutti, E.; Rizzo, G.; Mencarelli, A.; Orlandi, S.; Zanardo, R.; Renga, B.; Di Sante, M.; Morelli, A.; Cirino, G.; Wallace, J. L. Inhibition of Hydrogen Sulfide Generation Contributes to Gastric Injury Caused by Anti-Inflammatory Non-steroidal Drugs. *Gastroenterology* **2005**, *129*, 1210–1224.
- (17) Motta, J. P.; Flannigan, K. L.; Agbor, T. A.; Beatty, J. K.; Blackler, R. W.; Workentine, M. L.; Da Silva, G. J.; Wang, R.; Buret, A. G.; Wallace, J. L. Hydrogen Sulfide Protects from Colitis and Restores Intestinal Microbiota Biofilm and Mucus Production. *Inflamm Bowel Dis* **2015**, *21*, 1006–1017.
- (18) Wallace, J. L.; Vong, L.; McKnight, W.; Dickey, M.; Martin, G. R. Endogenous and Exogenous Hydrogen Sulfide Promotes Resolution of Colitis in Rats. *Gastroenterology* **2009**, *137*, S69–S78.e1.
- (19) Wallace, J. L.; Dickey, M.; McKnight, W.; Martin, G. R. Hydrogen Sulfide Enhances Ulcer Healing in Rats. *FASEB J.* **2007**, *21*, 4070–4076.
- (20) Mitchell, M. J.; Billingsley, M. M.; Haley, R. M.; Wechsler, M. E.; Peppas, N. A.; Langer, R. Engineering Precision Nanoparticles for Drug Delivery. *Nat. Rev. Drug Discovery* **2021**, *20*, 101–124.
- (21) Cifuentes-Rius, A.; Desai, A.; Yuen, D.; Johnston, A. P. R.; Voelcker, N. H. Inducing Immune Tolerance with Dendritic Cell-Targeting Nanomedicines. *Nat. Nanotechnol.* **2021**, *16*, 37–46.
- (22) Ramishetti, S.; Kedmi, R.; Goldsmith, M.; Leonard, F.; Sprague, A. G.; Godin, B.; Gozin, M.; Cullis, P. R.; Dykxhoorn, D. M.; Peer, D. Systemic Gene Silencing in Primary T Lymphocytes Using Targeted Lipid Nanoparticles. *ACS Nano* **2015**, *9*, 6706–6716.
- (23) Zhai, Y.; He, X.; Li, Y.; Han, R.; Ma, Y.; Gao, P.; Qian, Z.; Gu, Y.; Li, S. A Splenic-Targeted Versatile Antigen Courier: Ipsc Wrapped in Coalescent Erythrocyte-Liposome as Tumor Nanovaccine. *Sci. Adv.* **2021**, *7*, No. eabi6326.
- (24) Bronte, V.; Pittet, M. J. The Spleen in Local and Systemic Regulation of Immunity. *Immunity* **2013**, *39*, 806–818.
- (25) Schmid, D.; Park, C. G.; Hartl, C. A.; Subedi, N.; Cartwright, A. N.; Puerto, R. B.; Zheng, Y.; Maiarana, J.; Freeman, G. J.; Wucherpfennig, K. W.; Irvine, D. J.; Goldberg, M. S. T Cell-Targeting Nanoparticles Focus Delivery of Immunotherapy to Improve Antitumor Immunity. *Nat. Commun.* **2017**, *8*, 1747.
- (26) Huang, C. W.; Moore, P. K. H₂S Synthesizing Enzymes: Biochemistry and Molecular Aspects. *Handb Exp Pharmacol* **2015**, *230*, 3–25.
- (27) Ugliano, M.; Henschke, P. A. Comparison of Three Methods for Accurate Quantification of Hydrogen Sulfide During Fermentation. *Anal. Chim. Acta* **2010**, *660*, 87–91.
- (28) Miao, L.; Shen, X.; Whiteman, M.; Xin, H.; Shen, Y.; Xin, X.; Moore, P. K.; Zhu, Y. Z. Hydrogen Sulfide Mitigates Myocardial Infarction Via Promotion of Mitochondrial Biogenesis-Dependent M2 Polarization of Macrophages. *Antioxid Redox Signal* **2016**, *25*, 268–281.
- (29) Li, M.; Mao, J.; Zhu, Y. New Therapeutic Approaches Using Hydrogen Sulfide Donors in Inflammation and Immune Response. *Antioxid Redox Signal* **2021**, *35*, 341–356.
- (30) McWhorter, F. Y.; Wang, T.; Nguyen, P.; Chung, T.; Liu, W. F. Modulation of Macrophage Phenotype by Cell Shape. *Proc. Natl. Acad. Sci. U. S. A.* **2013**, *110*, 17253–17258.
- (31) Welch, M. J.; Hawker, C. J.; Wooley, K. L. The Advantages of Nanoparticles for PET. *J. Nucl. Med.* **2009**, *50*, 1743–1746.
- (32) Rauch, I.; Hainzl, E.; Rosebrock, F.; Heider, S.; Schwab, C.; Berry, D.; Stoiber, D.; Wagner, M.; Schleper, C.; Loy, A.; Urlich, T.; Muller, M.; Strobl, B.; Kenner, L.; Decker, T. Type I Interferons Have Opposing Effects During the Emergence and Recovery Phases of Colitis. *Eur. J. Immunol.* **2014**, *44*, 2749–2760.
- (33) Pasternak, B. A.; D'Mello, S.; Jurickova, I.; Han, X.; Willson, T.; Flick, L.; Petiniot, L.; Uozumi, N.; Divanovic, S.; Traurnicht, A.; Bonkowski, E.; Kugathasan, S.; Karp, C. L.; Denson, L. A. Lipopolysaccharide Exposure Is Linked to Activation of the Acute Phase Response and Growth Failure in Pediatric Crohn's Disease and Murine Colitis. *Inflamm Bowel Dis* **2010**, *16*, 856–869.
- (34) Guarner, F.; Malagelada, J. R. Role of Bacteria in Experimental Colitis. *Best Pract Res. Clin Gastroenterol* **2003**, *17*, 793–804.
- (35) Moparthi, L.; Koch, S. Wnt Signaling in Intestinal Inflammation. *Differentiation* **2019**, *108*, 24–32.
- (36) Wallace, J. L.; McKnight, W.; Asfaha, S.; Liu, D. Y. Reduction of Acute and Reactivated Colitis in Rats by an Inhibitor of Neutrophil Activation. *Am. J. Physiol.* **1998**, *274*, G802–G808.
- (37) Paul, S.; Shilpi, Lal, G. Role of Gamma-Delta (γδ) T Cells in Autoimmunity. *Pathobiology* **2015**, *97*, 259–271.
- (38) MacLeod, M. K.; Clambey, E. T.; Kappler, J. W.; Marrack, P. CD4Memory T Cells: What Are They and What Can They Do? *Semin Immunol* **2009**, *21*, 53–61.
- (39) Romagnani, S. Th1/Th2 Cells. *Inflamm Bowel Dis* **1999**, *5*, 285–294.
- (40) Liu, Z. J.; Yadav, P. K.; Su, J. L.; Wang, J. S.; Fei, K. Potential Role of Th17 Cells in the Pathogenesis of Inflammatory Bowel Disease. *World J. Gastroenterol* **2009**, *15*, 5784–5788.
- (41) Abe, K.; Nguyen, K. P.; Fine, S. D.; Mo, J. H.; Shen, C.; Shenouda, S.; Corr, M.; Jung, S.; Lee, J.; Eckmann, L.; Raz, E. Conventional Dendritic Cells Regulate the Outcome of Colonic Inflammation Independently of T Cells. *Proc. Natl. Acad. Sci. U. S. A.* **2007**, *104*, 17022–17027.
- (42) Ramirez, M.; Pell, N.; Mejias, M.; Fernandez, M. Pericytes in the Gut. *Adv. Exp. Med. Biol.* **2019**, *1122*, 73–100.
- (43) Zhang, G. Y.; Lu, D.; Duan, S. F.; Gao, Y. R.; Liu, S. Y.; Hong, Y.; Dong, P. Z.; Chen, Y. G.; Li, T.; Wang, D. Y.; Cheng, X. S.; He, F.; Wei, J. S.; Li, G. Y.; Zhang, Q. Y.; Wu, D. D.; Ji, X. Y. Hydrogen Sulfide Alleviates Lipopolysaccharide-Induced Diaphragm Dysfunction in Rats by Reducing Apoptosis and Inflammation through Ros/Mapk and TLR4/NF-KappaB Signaling Pathways. *Oxid Med. Cell Longev* **2018**, *2018*, 15.
- (44) Xu, W.; Chen, J.; Lin, J.; Liu, D.; Mo, L.; Pan, W.; Feng, J.; Wu, W.; Zheng, D. Exogenous H₂S Protects H9c2 Cardiac Cells against High Glucose-Induced Injury and Inflammation by Inhibiting the Activation of the NF-KappaB and IL-1beta Pathways. *Int. J. Mol. Med.* **2015**, *35*, 177–186.
- (45) Chassaing, B.; Aitken, J. D.; Malleshappa, M.; Vijay-Kumar, M. Dextran Sulfate Sodium (DSS)-Induced Colitis in Mice. *Curr. Protoc Immunol* **2014**, *104*, 15.25.1–15.25.14.
- (46) Johansson, M. E.; Gustafsson, J. K.; Holmen-Larsson, J.; Jabbar, K. S.; Xia, L.; Xu, H.; Ghishan, F. K.; Carvalho, F. A.; Gewirtz, A. T.; Sjövall, H.; Hansson, G. C. Bacteria Penetrate the Normally

- Impenetrable Inner Colon Mucus Layer in Both Murine Colitis Models and Patients with Ulcerative Colitis. *Gut* **2014**, *63*, 281–291.
- (47) Morgan, M. E.; Zheng, B.; Koelink, P. J.; van de Kant, H. J.; Haazen, L. C.; van Roest, M.; Garssen, J.; Folkerts, G.; Kraneveld, A. D. New Perspective on Dextran Sodium Sulfate Colitis: Antigen-Specific T Cell Development During Intestinal Inflammation. *PLoS One* **2013**, *8*, No. e69936.
- (48) Hall, L. J.; Faivre, E.; Quinlan, A.; Shanahan, F.; Nally, K.; Melgar, S. Induction and Activation of Adaptive Immune Populations During Acute and Chronic Phases of a Murine Model of Experimental Colitis. *Dig. Dis. Sci.* **2011**, *56*, 79–89.
- (49) Szabo, C. Gasotransmitters in Cancer: From Pathophysiology to Experimental Therapy. *Nat. Rev. Drug Discov* **2016**, *15*, 185–203.
- (50) Wang, R. Gasotransmitters: Growing Pains and Joys. *Trends Biochem. Sci.* **2014**, *39*, 227–232.
- (51) Flannigan, K. L.; Agbor, T. A.; Blackler, R. W.; Kim, J. J.; Khan, W. L.; Verdu, E. F.; Ferraz, J. G.; Wallace, J. L. Impaired Hydrogen Sulfide Synthesis and IL-10 Signaling Underlie Hyperhomocysteinemia-Associated Exacerbation of Colitis. *Proc. Natl. Acad. Sci. U. S. A.* **2014**, *111*, 13559–13564.
- (52) Hirata, I.; Naito, Y.; Takagi, T.; Mizushima, K.; Suzuki, T.; Omatsu, T.; Handa, O.; Ichikawa, H.; Ueda, H.; Yoshikawa, T. Endogenous Hydrogen Sulfide Is an Anti-Inflammatory Molecule in Dextran Sodium Sulfate-Induced Colitis in Mice. *Dig. Dis. Sci.* **2011**, *56* (5), 1379–1386.
- (53) De Cicco, P.; Sanders, T.; Cirino, G.; Maloy, K. J.; Ianaro, A. Hydrogen Sulfide Reduces Myeloid-Derived Suppressor Cell-Mediated Inflammatory Response in a Model of Helicobacter Hepaticus-Induced Colitis. *Front. Immunol.* **2018**, *9*, 499.
- (54) Chen, S.; Zuo, S.; Zhu, J.; Yue, T.; Bu, D.; Wang, X.; Wang, P.; Pan, Y.; Liu, Y. Decreased Expression of Cystathionine Beta-Synthase Exacerbates Intestinal Barrier Injury in Ulcerative Colitis. *J. Crohns Colitis* **2019**, *13*, 1067–1080.
- (55) Hegazi, R. A.; Rao, K. N.; Mayle, A.; Sepulveda, A. R.; Otterbein, L. E.; Plevy, S. E. Carbon Monoxide Ameliorates Chronic Murine Colitis through a Heme Oxygenase 1-Dependent Pathway. *J. Exp. Med.* **2005**, *202*, 1703–1713.
- (56) Byrne, J. D.; Gallo, D.; Boyce, H.; Becker, S. L.; Kezar, K. M.; Cotoia, A. T.; Feig, V. R.; Lopes, A.; Csizmadia, E.; Longhi, M. S.; Lee, J. S.; Kim, H.; Wentworth, A. J.; Shankar, S.; Lee, G. R.; Bi, J.; Witt, E.; Ishida, K.; Hayward, A.; Kuosmanen, J. L. P.; et al. Delivery of Therapeutic Carbon Monoxide by Gas-Entrapping Materials. *Sci. Transl. Med.* **2022**, *14*, No. eabl4135.
- (57) Rachmilewitz, D.; Stampler, J. S.; Bachwich, D.; Karmeli, F.; Ackerman, Z.; Podolsky, D. K. Enhanced Colonic Nitric Oxide Generation and Nitric Oxide Synthase Activity in Ulcerative Colitis and Crohn's Disease. *Gut* **1995**, *36*, 718–723.
- (58) Middleton, S. J.; Shorthouse, M.; Hunter, J. O. Increased Nitric Oxide Synthase in Ulcerative Colitis. *Lancet* **1993**, *341*, 465–466.
- (59) Zhang, G.; Wang, P.; Yang, G.; Cao, Q.; Wang, R. The Inhibitory Role of Hydrogen Sulfide in Airway Hyperresponsiveness and Inflammation in a Mouse Model of Asthma. *Am. J. Pathol.* **2013**, *182*, 1188–1195.
- (60) Li, L.; Fox, B.; Keeble, J.; Salto-Tellez, M.; Winyard, P. G.; Wood, M. E.; Moore, P. K.; Whiteman, M. The Complex Effects of the Slow-Releasing Hydrogen Sulfide Donor GYY4137 in a Model of Acute Joint Inflammation and in Human Cartilage Cells. *J. Cell Mol. Med.* **2013**, *17*, 365–376.
- (61) Wallace, J. L.; Ferraz, J. G.; Muscara, M. N. Hydrogen Sulfide: An Endogenous Mediator of Resolution of Inflammation and Injury. *Antioxid. Redox Signal* **2012**, *17*, 58–67.
- (62) Yang, R.; Qu, C.; Zhou, Y.; Konkol, J. E.; Shi, S.; Liu, Y.; Chen, C.; Liu, S.; Liu, D.; Chen, Y.; Zandi, E.; Chen, W.; Zhou, Y.; Shi, S. Hydrogen Sulfide Promotes Tet1- and Tet2-Mediated Foxp3 Demethylation to Drive Regulatory T Cell Differentiation and Maintain Immune Homeostasis. *Immunity* **2015**, *43*, 251–263.
- (63) Erben, U.; Lodenkemper, C.; Doerfel, K.; Spieckermann, S.; Haller, D.; Heimesaat, M. M.; Zeitz, M.; Siegmund, B.; Kuhl, A. A. A Guide to Histomorphological Evaluation of Intestinal Inflammation in Mouse Models. *Int. J. Clin. Exp. Pathol.* **2014**, *7*, 4557–4576.
- (64) de Araujo, A.; de Lartigue, G. Non-Canonical Cholinergic Anti-Inflammatory Pathway in *Ibd*. *Nat. Rev. Gastroenterol. Hepatol.* **2020**, *17*, 651–652.
- (65) Boehm, F.; Martin, M.; Kesselring, R.; Schiechl, G.; Geissler, E. K.; Schlitt, H. J.; Fichtner-Feigl, S. Deletion of Foxp3+ Regulatory T Cells in Genetically Targeted Mice Supports Development of Intestinal Inflammation. *BMC Gastroenterol.* **2012**, *12*, 97.
- (66) Veltkamp, C.; Anstaett, M.; Wahl, K.; Moller, S.; Gangl, S.; Bachmann, O.; Hardtke-Wolenski, M.; Langer, F.; Stremmel, W.; Manns, M. P.; Schulze-Osthoff, K.; Bantel, H. Apoptosis of Regulatory T Lymphocytes Is Increased in Chronic Inflammatory Bowel Disease and Reversed by Anti-Tnfalpha Treatment. *Gut* **2011**, *60*, 1345–1353.
- (67) Teratani, T.; Mikami, Y.; Nakamoto, N.; Suzuki, T.; Harada, Y.; Okabayashi, K.; Hagihara, Y.; Taniki, N.; Kohno, K.; Shibata, S.; Miyamoto, K.; Ishigame, H.; Chu, P. S.; Sujino, T.; Suda, W.; Hattori, M.; Matsui, M.; Okada, T.; Okano, H.; Inoue, M.; et al. The Liver-Brain-Gut Neural Arc Maintains the Treg Cell Niche in the Gut. *Nature* **2020**, *585*, 591–596.
- (68) Kanamori, M.; Nakatsukasa, H.; Okada, M.; Lu, Q.; Yoshimura, A. Induced Regulatory T Cells: Their Development, Stability, and Applications. *Trends Immunol.* **2016**, *37*, 803–811.
- (69) Mebius, R. E.; Kraal, G. Structure and Function of the Spleen. *Nat. Rev. Immunol.* **2005**, *5*, 606–616.
- (70) Humphrey, J. H.; Grennan, D. Different Macrophage Populations Distinguished by Means of Fluorescent Polysaccharides. Recognition and Properties of Marginal-Zone Macrophages. *Eur. J. Immunol.* **1981**, *11*, 221–228.
- (71) Yamazaki, S.; Dudziak, D.; Heidkamp, G. F.; Fiorese, C.; Bonito, A. J.; Inaba, K.; Nussenzweig, M. C.; Steinman, R. M. CD8+ CD205+ Splenic Dendritic Cells Are Specialized to Induce Foxp3+ Regulatory T Cells. *J. Immunol.* **2008**, *181*, 6923–6933.
- (72) Seifert, H. A.; Hall, A. A.; Chapman, C. B.; Collier, L. A.; Willing, A. E.; Pennypacker, K. R. A Transient Decrease in Spleen Size Following Stroke Corresponds to Splenocyte Release into Systemic Circulation. *J. Neuroimmune Pharmacol.* **2012**, *7*, 1017–1024.
- (73) Heusch, G. The Spleen in Myocardial Infarction. *Circ. Res.* **2019**, *124*, 26–28.
- (74) Feng, Z.; Wang, R.; Wang, G.; Wang, C.; Tan, Y.; Liu, L.; Wang, C.; Liu, Y.; et al. The Novel Severe Acute Respiratory Syndrome Coronavirus 2 (SARS-Cov-2) Directly Decimates Human Spleens and Lymph Nodes. *BIO-PROTOCOL* **2020**, *10* DOI: 10.21769/BioProtoc.5002 (accessed March 31, 2020).
- (75) Swirski, F. K.; Nahrendorf, M.; Etzrodt, M.; Wildgruber, M.; Cortez-Retamozo, V.; Panizzi, P.; Figueiredo, J. L.; Kohler, R. H.; Chudnovskiy, A.; Waterman, P.; Aikawa, E.; Mempel, T. R.; Libby, P.; Weissleder, R.; Pittet, M. J. Identification of Splenic Reservoir Monocytes and Their Deployment to Inflammatory Sites. *Science* **2009**, *325*, 612–616.
- (76) Getts, D. R.; Turley, D. M.; Smith, C. E.; Harp, C. T.; McCarthy, D.; Feeney, E. M.; Getts, M. T.; Martin, A. J.; Luo, X.; Terry, R. L.; King, N. J.; Miller, S. D. Tolerance Induced by Apoptotic Antigen-Coupled Leukocytes Is Induced by PD-L1+ and IL-10-Producing Splenic Macrophages and Maintained by T Regulatory Cells. *J. Immunol.* **2011**, *187*, 2405–2417.
- (77) Zachs, D. P.; Offutt, S. J.; Graham, R. S.; Kim, Y.; Mueller, J.; Auger, J. L.; Schuldt, N. J.; Kaiser, C. R. W.; Heiller, A. P.; Dutta, R.; Guo, H.; Alford, J. K.; Binstadt, B. A.; Lim, H. H. Noninvasive Ultrasound Stimulation of the Spleen to Treat Inflammatory Arthritis. *Nat. Commun.* **2019**, *10*, 951.
- (78) Kaur, S.; Allan, S. M.; Al-Ahmady, Z. S. Re-Directing Nanomedicines to the Spleen: A Potential Technology for Peripheral Immunomodulation. *J. Controlled Release* **2022**, *350*, 60–79.
- (79) Chen, K. H.; Lundy, D. J.; Toh, E. K.; Chen, C. H.; Shih, C.; Chen, P.; Chang, H. C.; Lai, J. J.; Stayton, P. S.; Hoffman, A. S.; Hsieh, P. C. Nanoparticle Distribution During Systemic Inflammation

- Is Size-Dependent and Organ-Specific. *Nanoscale* **2015**, *7*, 15863–15872.
- (80) Aichele, P.; Zinke, J.; Grode, L.; Schwendener, R. A.; Kaufmann, S. H.; Seiler, P. Macrophages of the Splenic Marginal Zone Are Essential for Trapping of Blood-Borne Particulate Antigen but Dispensable for Induction of Specific T Cell Responses. *J. Immunol* **2003**, *171*, 1148–1155.
- (81) Harasym, T. O.; Tardi, P.; Longman, S. A.; Ansell, S. M.; Bally, M. B.; Cullis, P. R.; Choi, L. S. Poly(Ethylene Glycol)-Modified Phospholipids Prevent Aggregation During Covalent Conjugation of Proteins to Liposomes. *Bioconjug Chem.* **1995**, *6*, 187–194.
- (82) Shimizu, T.; Abu Lila, A. S.; Kawaguchi, Y.; Shimazaki, Y.; Watanabe, Y.; Mima, Y.; Hashimoto, Y.; Okuhira, K.; Storm, G.; Ishima, Y.; Ishida, T. A Novel Platform for Cancer Vaccines: Antigen-Selective Delivery to Splenic Marginal Zone B Cells Via Repeated Injections of Pegylated Liposomes. *J. Immunol* **2018**, *201*, 2969–2976.
- (83) Tripathi, P.; Dwivedi, P.; Khatik, R.; Jaiswal, A. K.; Dube, A.; Shukla, P.; Mishra, P. R. Development of 4-Sulfated N-Acetyl Galactosamine Anchored Chitosan Nanoparticles: A Dual Strategy for Effective Management of Leishmaniasis. *Colloids Surf. B Biointerfaces* **2015**, *136*, 150–159.
- (84) Ye, J.; Wang, Q.; Zhou, X.; Zhang, N. Injectable Actarit-Loaded Solid Lipid Nanoparticles as Passive Targeting Therapeutic Agents for Rheumatoid Arthritis. *Int. J. Pharm.* **2008**, *352*, 273–279.
- (85) Yi, S.; Allen, S. D.; Liu, Y. G.; Ouyang, B. Z.; Li, X.; Augornworawat, P.; Thorp, E. B.; Scott, E. A. Tailoring Nanostructure Morphology for Enhanced Targeting of Dendritic Cells in Atherosclerosis. *ACS Nano* **2016**, *10*, 11290–11303.
- (86) Kranz, L. M.; Diken, M.; Haas, H.; Kreiter, S.; Loquai, C.; Reuter, K. C.; Meng, M.; Fritz, D.; Vascotto, F.; Hefesha, H.; Grunwitz, C.; Vormehr, M.; Husemann, Y.; Selmi, A.; Kuhn, A. N.; Buck, J.; Derhovanessian, E.; Rae, R.; Attig, S.; Diekmann, J.; et al. Systemic RNA Delivery to Dendritic Cells Exploits Antiviral Defence for Cancer Immunotherapy. *Nature* **2016**, *534*, 396–401.
- (87) Li, L.; Whiteman, M.; Guan, Y. Y.; Neo, K. L.; Cheng, Y.; Lee, S. W.; Zhao, Y.; Baskar, R.; Tan, C. H.; Moore, P. K. Characterization of a Novel, Water-Soluble Hydrogen Sulfide-Releasing Molecule (GYY4137): New Insights into the Biology of Hydrogen Sulfide. *Circulation* **2008**, *117*, 2351–2360.
- (88) Lee, Z. W.; Zhou, J.; Chen, C. S.; Zhao, Y.; Tan, C. H.; Li, L.; Moore, P. K.; Deng, L. W. The Slow-Releasing Hydrogen Sulfide Donor, GYY4137, Exhibits Novel Anti-Cancer Effects in Vitro and in Vivo. *PLoS One* **2011**, *6*, No. e21077.
- (89) Sasakura, K.; Hanaoka, K.; Shibuya, N.; Mikami, Y.; Kimura, Y.; Komatsu, T.; Ueno, T.; Terai, T.; Kimura, H.; Nagano, T. Development of a Highly Selective Fluorescence Probe for Hydrogen Sulfide. *J. Am. Chem. Soc.* **2011**, *133*, 18003–18005.
- (90) Sakuma, S.; Minamino, S.; Takase, M.; Ishiyama, Y.; Hosokura, H.; Kohda, T.; Ikeda, Y.; Fujimoto, Y. Hydrogen Sulfide Donor GYY4137 Suppresses Proliferation of Human Colorectal Cancer Caco-2 Cells by Inducing Both Cell Cycle Arrest and Cell Death. *Heliyon* **2019**, *5*, No. e02244.
- (91) Park, J.; Choi, J.; Lee, J. E.; Choi, H.; Im, H. J. Spatial Transcriptomics-Based Identification of Molecular Markers for Nanomedicine Distribution in Tumor Tissue. *Small Methods* **2022**, *6*, No. e2201091.
- (92) Ocampo, S. M.; Romero, C.; Avino, A.; Burgueno, J.; Gassull, M. A.; Bermudez, J.; Eritja, R.; Fernandez, E.; Perales, J. C. Functionally Enhanced Sirna Targeting Tnfalpha Attenuates Dss-Induced Colitis and TLR-Mediated Immunostimulation in Mice. *Mol. Ther* **2012**, *20*, 382–390.
- (93) Planell, N.; Lozano, J. J.; Mora-Buch, R.; Masamunt, M. C.; Jimeno, M.; Ordas, I.; Esteller, M.; Ricart, E.; Pique, J. M.; Panes, J.; Salas, A. Transcriptional Analysis of the Intestinal Mucosa of Patients with Ulcerative Colitis in Remission Reveals Lasting Epithelial Cell Alterations. *Gut* **2013**, *62*, 967–976.
- (94) Wirtz, S.; Popp, V.; Kindermann, M.; Gerlach, K.; Weigmann, B.; Fichtner-Feigl, S.; Neurath, M. F. Chemically Induced Mouse

Models of Acute and Chronic Intestinal Inflammation. *Nat. Protoc* **2017**, *12*, 1295–1309.

(95) Zhao, H.; Yan, R.; Zhou, X.; Ji, F.; Zhang, B. Hydrogen Sulfide Improves Colonic Barrier Integrity in DSS-Induced Inflammation in Caco-2 Cells and Mice. *Int. Immunopharmacol* **2016**, *39*, 121–127.

(96) Perse, M.; Cerar, A. Dextran Sodium Sulphate Colitis Mouse Model: Traps and Tricks. *J. Biomed. Biotechnol.* **2012**, *2012*, 718617.

(97) Schubert, M.; Klinger, B.; Klunemann, M.; Sieber, A.; Uhlig, F.; Sauer, S.; Garnett, M. J.; Bluthgen, N.; Saez-Rodriguez, J. Perturbation-Response Genes Reveal Signaling Footprints in Cancer Gene Expression. *Nat. Commun.* **2018**, *9*, 20.

Recommended by ACS

Nitric Oxide-Loaded Bioinspired Lipoprotein Normalizes Tumor Vessels To Improve Intratumor Delivery and Chemotherapy of Albumin-Bound Paclitaxel Nanoparticles

Yao Wu, Zhiwen Zhang, et al.

JANUARY 26, 2023
NANO LETTERS

READ 

Dual-Targeted Nanodiscs Revealing the Cross-Talk between Osteogenic Differentiation of Mesenchymal Stem Cells and Macrophages

Lang Chen, Guohui Liu, et al.

JANUARY 30, 2023
ACS NANO

READ 

A Cascade Targeted and Mitochondrion-Dysfunctional Nanomedicine Capable of Overcoming Drug Resistance in Hepatocellular Carcinoma

Yuanyuan Yang, Zhiqiang Yu, et al.

JANUARY 05, 2023
ACS NANO

READ 

Augmenting Intracellular Cargo Delivery of Extracellular Vesicles in Hypoxic Tissues through Inhibiting Hypoxia-Induced Endocytic Recycling

Bide Tong, Cao Yang, et al.

FEBRUARY 02, 2023
ACS NANO

READ 

Get More Suggestions >